Supplement of Atmos. Meas. Tech., 11, 3717–3735, 2018
https://doi.org/10.5194/amt-11-3717-2018-supplement

Atmospheric Measurement Techniques
Open Access
EGU

Supplement of

Performance of NO, NO_2 low cost sensors and three calibration approaches within a real world application

Alessandro Bigi et al.

Correspondence to: Alessandro Bigi (alessandro.bigi@unimore.it)

month	NO (ppb)	NO_2 (ppb)	T (^oC)	RH (%)
		Härkingen		
4	14.7 (<LOD – 218.3)	17.0 (1.1 – 75.9)	9.5 (-2.3 – 24.5)	64.0 (18.8 – 96.6)
5	13.8 (<LOD – 190.6)	16.4 (0.9 – 60.4)	15.2 (2.3 – 32.1)	67.7 (24.8 – 94.7)
6	13.0 (<LOD – 143.6)	17.0 (1.0 – 57.5)	20.6 (6.4 – 33.9)	64.0 (22.0 – 90.9)
7	15.1 (<LOD – 128.1)	15.5 (1.1 – 55.9)	18.6 (11.8 – 30.6)	70.4 (37.2 – 91.0)
		Zurich		
8	2.5 (<LOD – 53.7)	11.6 (0.0 – 43.6)	21.5 (12.2 – 33)	66.9 (28.9 – 92.6)
9	4.7 (<LOD – 102.9)	12.7 (1.4 – 51.1)	14.8 (7.0 – 25.8)	70.9 (37.2 – 94.0)
10	11.8 (<LOD – 164.3)	17 (1.6 – 52.2)	12.7 (2.5 – 23.3)	72.7 (24.9 – 98)
11	11 (<LOD – 135.7)	16.6 (2.1 – 46.3)	6.4 (0.4 – 17.2)	75.2 (36 – 92.9)
		Lausanne		
8	10.4 (<LOD – 109.2)	19.1 (1.1 – 69.7)	21.8 (12.6 – 34.9)	60.3 (27.7 – 90.5)
9	14.0 (<LOD – 266.5)	19.4 (1.2 – 71.2)	15.2 (8.7 – 25.8)	65.9 (31.5 – 87.8)
10	17.5 (0.2 – 178.8)	21.1 (1.1 – 64.6)	13.2 (3.8 – 21.1)	66.2 (34.4 – 89)
11	18.2 (0.4 – 201.1)	19.5 (1.2 – 67.7)	6.4 (0.5 – 15.2)	70.7 (38.6 – 90.3)

Table S1: Monthly summary statistics for the calibration and deployment sites. Mean and range (within brackets) are shown for all investigated months. LOD for NO reference instruments is ca. 0.2 ppb

	NO															
	MAE (ppb)				MBE (ppb)				R^2 –				RMSE (ppb)			
	Minimal	Basic	S. Repl.	D. Repl.	Minimal	Basic	S. Repl.	D. Repl.	Minimal	Basic	S. Repl.	D. Repl.	Minimal	Basic	S. Repl.	D. Repl.
MLR	4.6 ± 1.0	4.3 ± 0.9	4.4 ± 1.1	4.6 ± 0.9	-0.5 ± 1.5	-0.1 ± 0.8	-1.1 ± 1.4	-1.3 ± 1.3	0.84 ± 0.06	0.86 ± 0.05	0.84 ± 0.07	0.85 ± 0.05	6.7 ± 1.6	6.2 ± 1.6	6.6 ± 2.1	6.4 ± 1.7
SVR	3.7 ± 1.0	3.1 ± 0.8	3.8 ± 1.2	3.4 ± 0.9	-0.4 ± 1.9	0.1 ± 1.2	-0.3 ± 2.1	0.5 ± 1.4	0.88 ± 0.07	0.91 ± 0.05	0.87 ± 0.07	0.90 ± 0.05	5.7 ± 2.3	5.1 ± 2.0	5.9 ± 2.5	5.3 ± 2.0
RF	3.7 ± 1.1	3.0 ± 1.0	3.8 ± 1.2	3.0 ± 1.0	-0.5 ± 1.8	-0.4 ± 1.0	-0.6 ± 1.9	-0.4 ± 1.0	0.87 ± 0.06	0.91 ± 0.05	0.87 ± 0.07	0.90 ± 0.05	5.9 ± 2.3	5.1 ± 2.2	5.9 ± 2.3	5.2 ± 2.1

	NO_2															
	MAE (ppb)				MBE (ppb)				R^2 –				RMSE (ppb)			
	Minimal	Basic	S. Repl.	D. Repl.	Minimal	Basic	S. Repl.	D. Repl.	Minimal	Basic	S. Repl.	D. Repl.	Minimal	Basic	S. Repl.	D. Repl.
MLR	4.6 ± 1.3	4.4 ± 1.1	4.3 ± 1.1	4.3 ± 0.4	-0.2 ± 0.5	-1.1 ± 0.2	0.6 ± 0.6	-0.8 ± 0.2	0.66 ± 0.17	0.69 ± 0.16	0.70 ± 0.12	0.71 ± 0.08	5.8 ± 1.5	5.5 ± 1.4	5.5 ± 1.3	5.4 ± 0.5
SVR	4.1 ± 0.9	3.4 ± 0.6	4.2 ± 0.5	3.2 ± 0.6	-1.0 ± 1.2	-0.6 ± 1.0	0.0 ± 0.8	-0.6 ± 0.7	0.72 ± 0.10	0.79 ± 0.06	0.71 ± 0.06	0.82 ± 0.06	5.3 ± 1.0	4.5 ± 0.6	5.4 ± 0.5	4.2 ± 0.9
RF	4.4 ± 0.9	3.3 ± 0.9	4.1 ± 0.5	3.1 ± 0.7	-0.1 ± 1.0	-0.7 ± 0.8	0.3 ± 0.9	-0.5 ± 0.6	0.69 ± 0.11	0.81 ± 0.09	0.73 ± 0.04	0.84 ± 0.05	5.5 ± 1.0	4.3 ± 1.1	5.2 ± 0.6	4.0 ± 0.9

Table S2: Comparison of algorithms' perfomance using the 4 main models in Appendix A in the main manuscript. Mean value ± standard deviation for each index are shown. MAE stands for Mean Absolute Error, MBE for Mean Bias Error, R^2 for the coefficient of determination and RMSE for the root mean of square errors.

Algorithm	MAE (ppb)	MBE (ppb)	R^2 –	RMSE (ppb)
		NO		
RF	3.0 ± 0.9	-0.3 ± 1.1	0.91 ± 0.04	5.0 ± 2.0
		NO_2		
RF	2.7 ± 0.8	-0.2 ± 0.5	0.89 ± 0.03	3.4 ± 1.1

Table S3: Performance of a RF model using both SUs for each site, i.e. 8 EC sensors (see the main manuscript). Mean value ± standard deviation for each index are shown. MAE stands for Mean Absolute Error, MBE for Mean Bias Error, R^2 for the coefficient of determination and RMSE for the root mean of square errors.

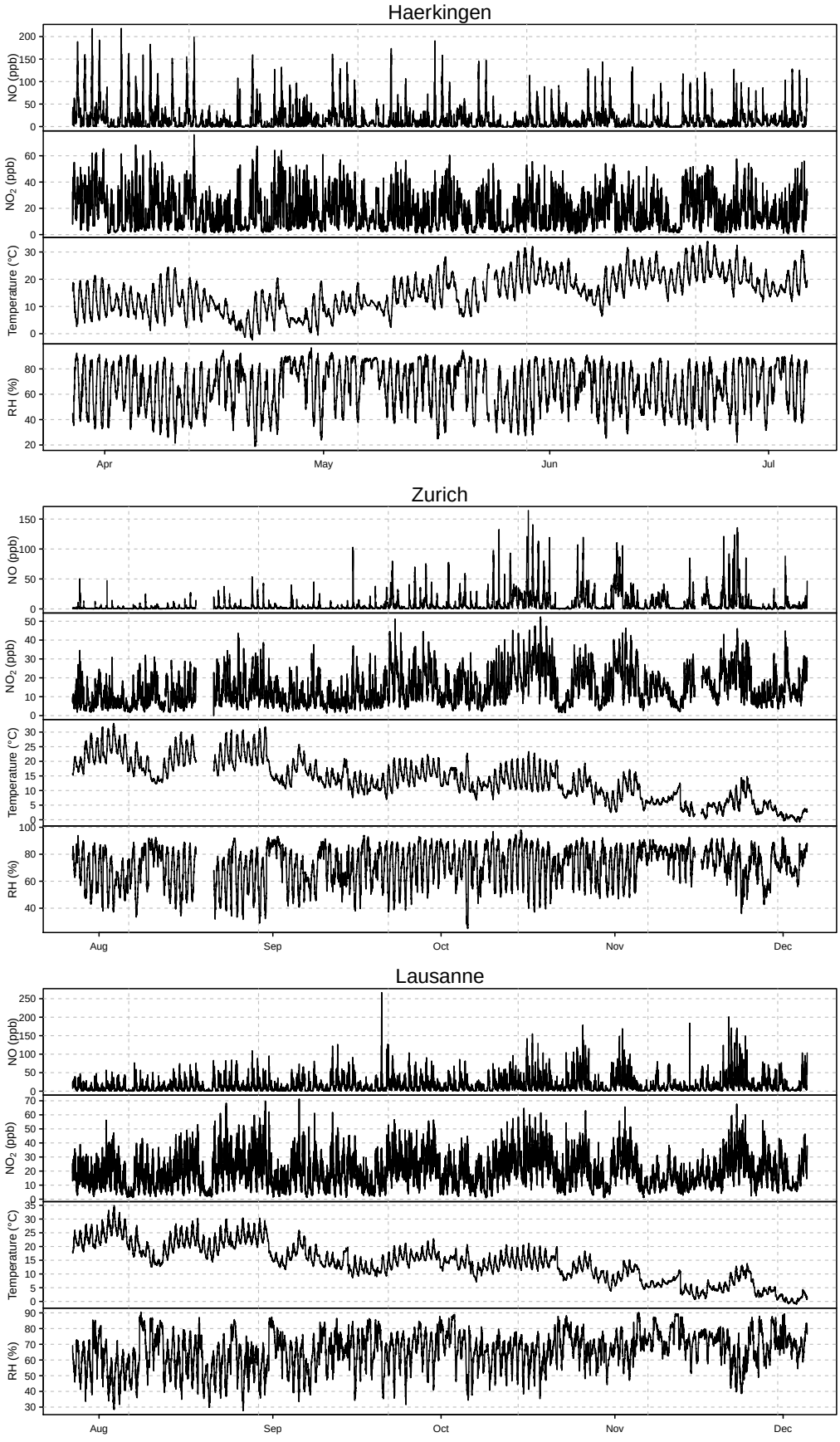

Figure S1: Time series of data collected at the Härkingen, Zurich and Lausanne reference sites.

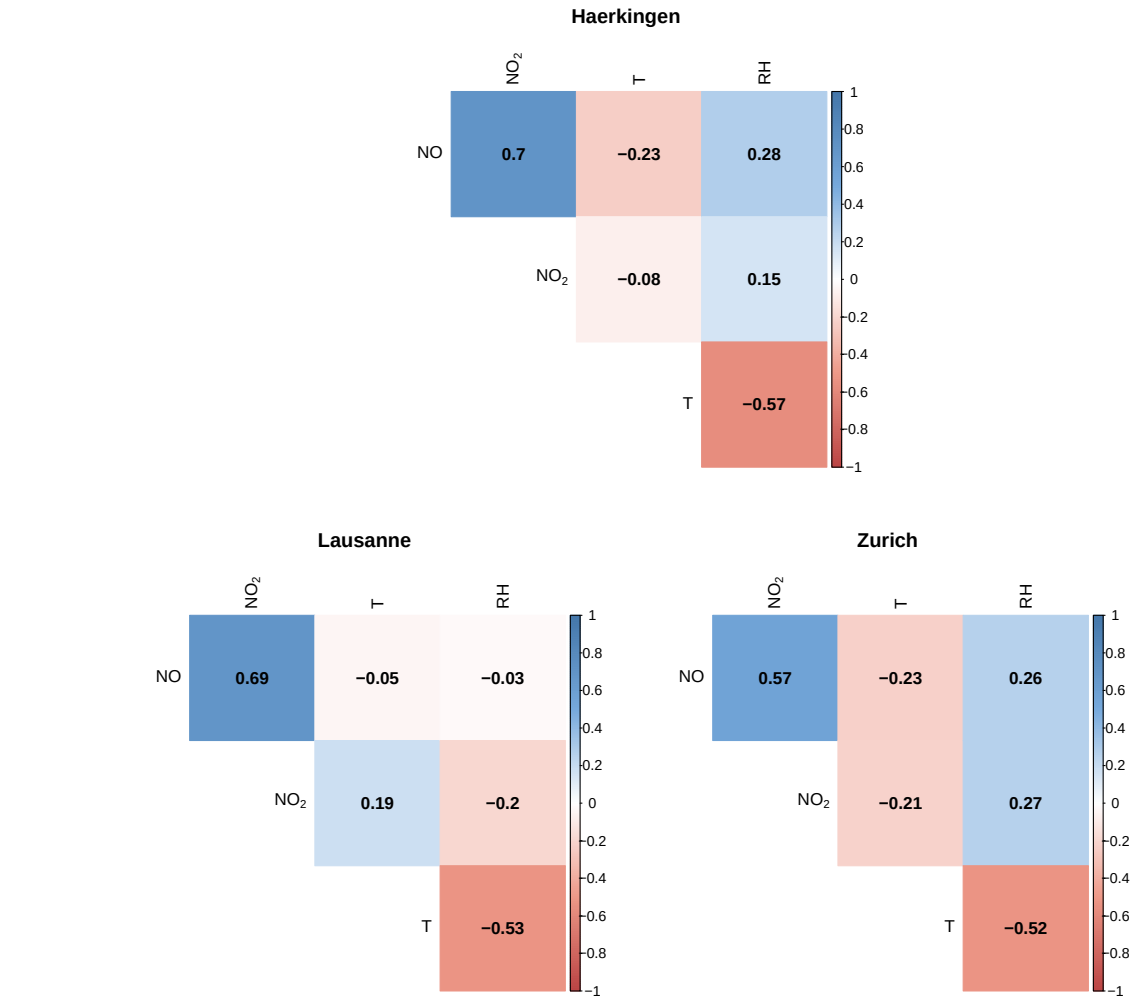

Figure S2: Correlation matrix for meterological variables and pollutant concentration at the calibration and deployment sites.

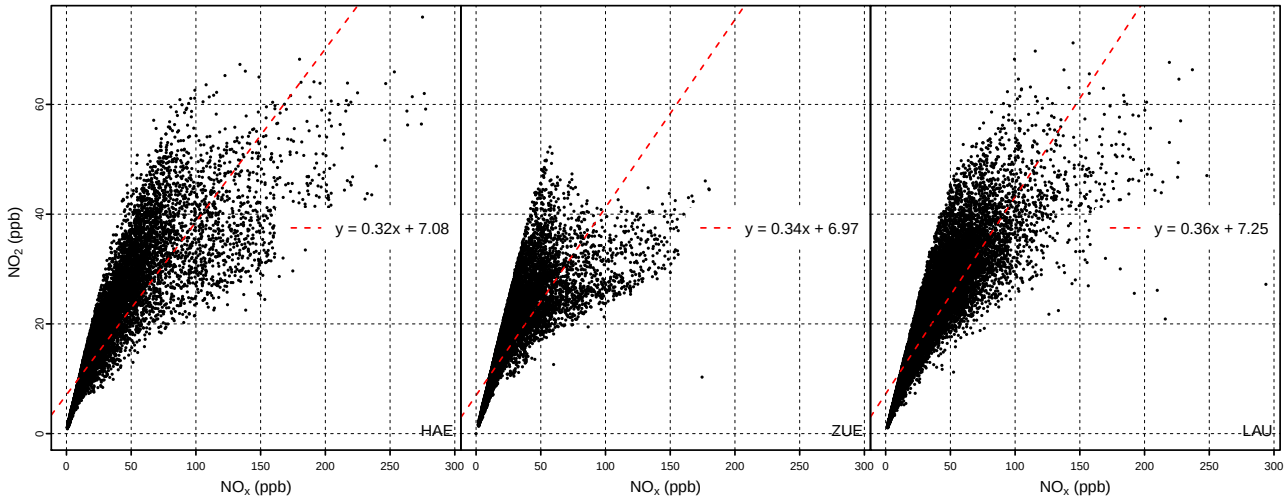

Figure S3: Scatterplot of NO_2 and NO_x at the three sites. Red dashed line indicates the linear regression model.

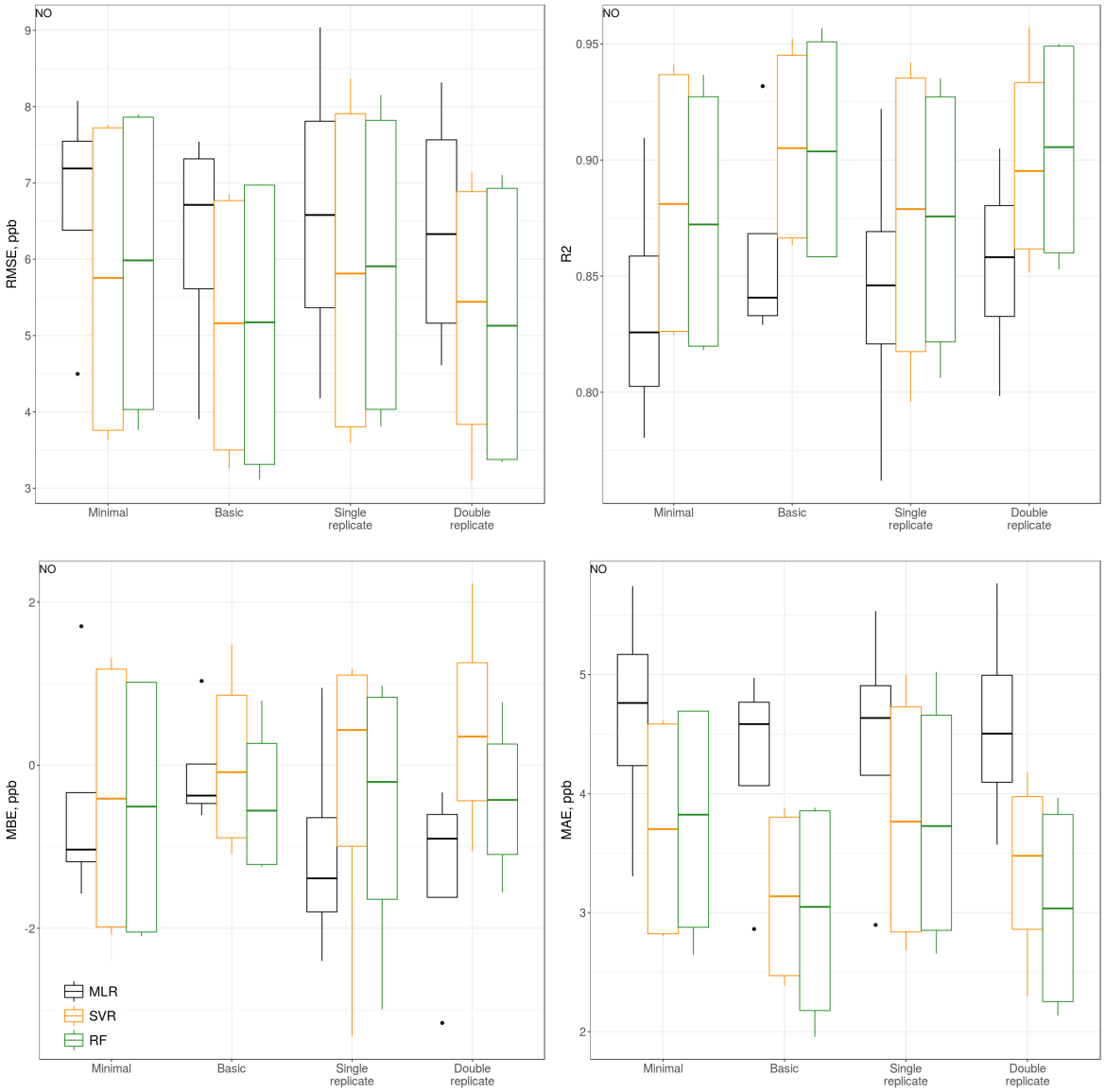

Figure S4: Comparison of goodness-of-fit indexes for the 4 main models listed in Appendix A for the prediction of NO.

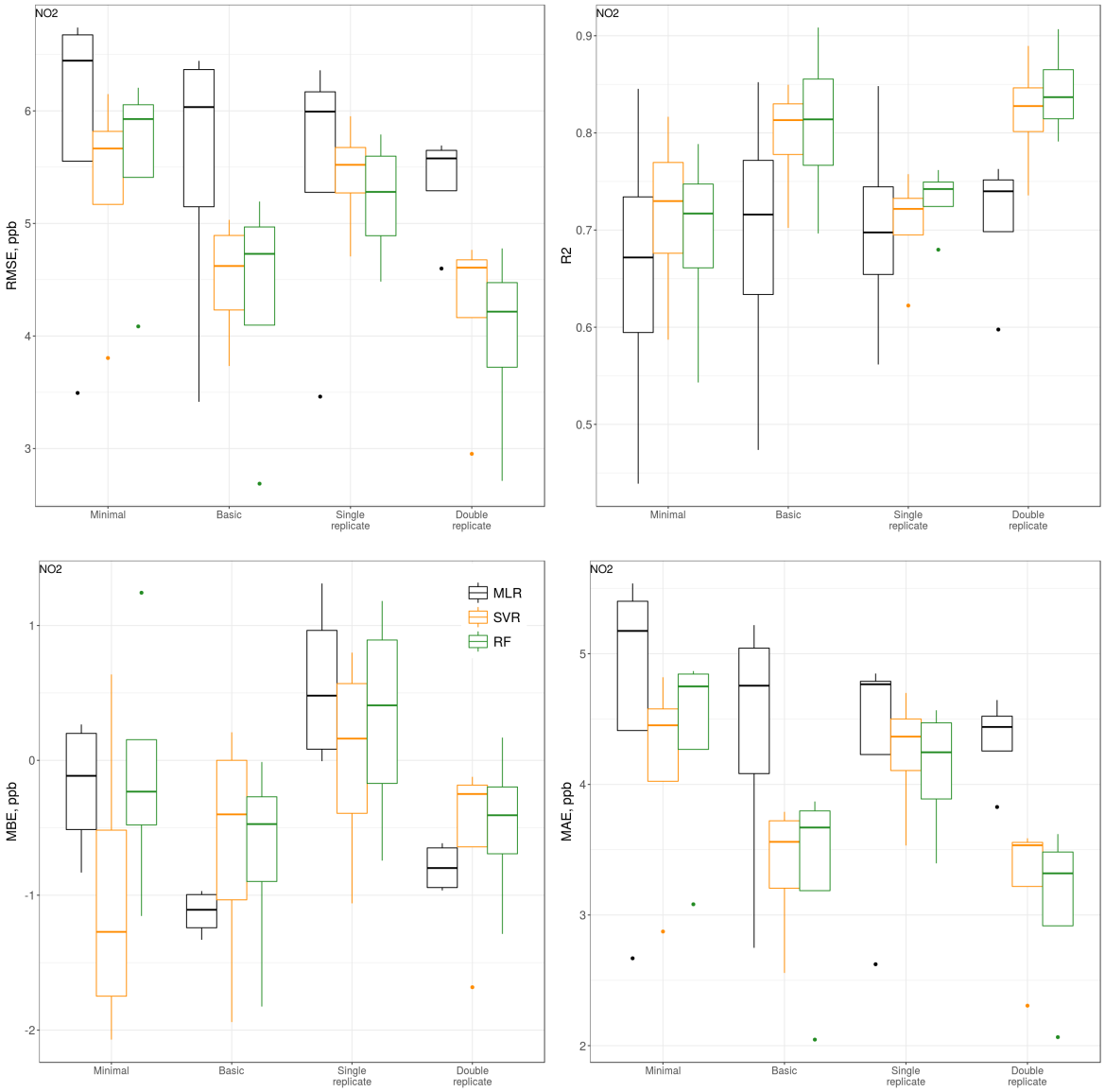

Figure S5: Comparison of goodness-of-fit indexes for the 4 main models listed in Appendix A for the prediction of NO_2.

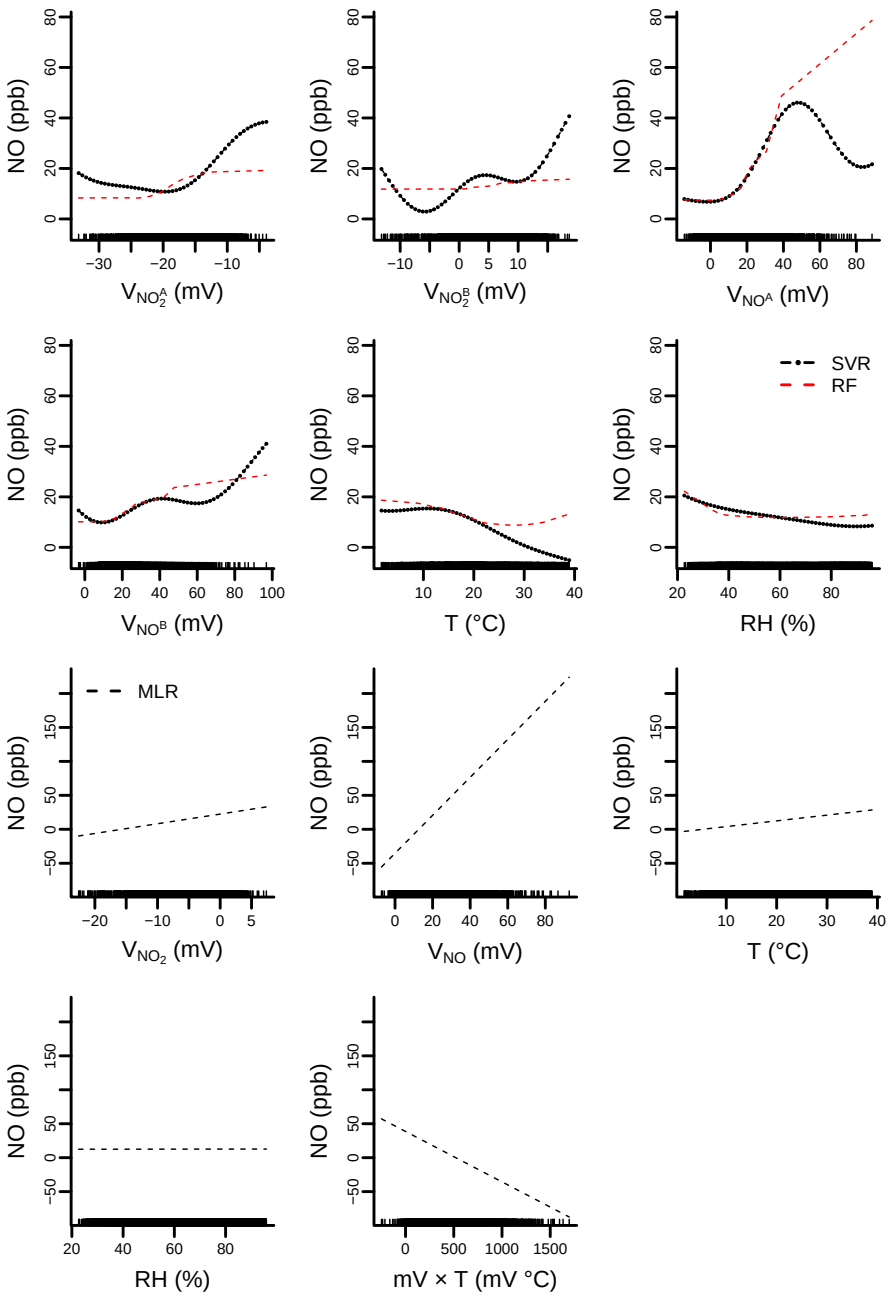

Figure S6: Partial plots for SVM, RF and MLR for the calibration dataset from SU010, NO. Rug on the abscissa indicates the range of the covariate.

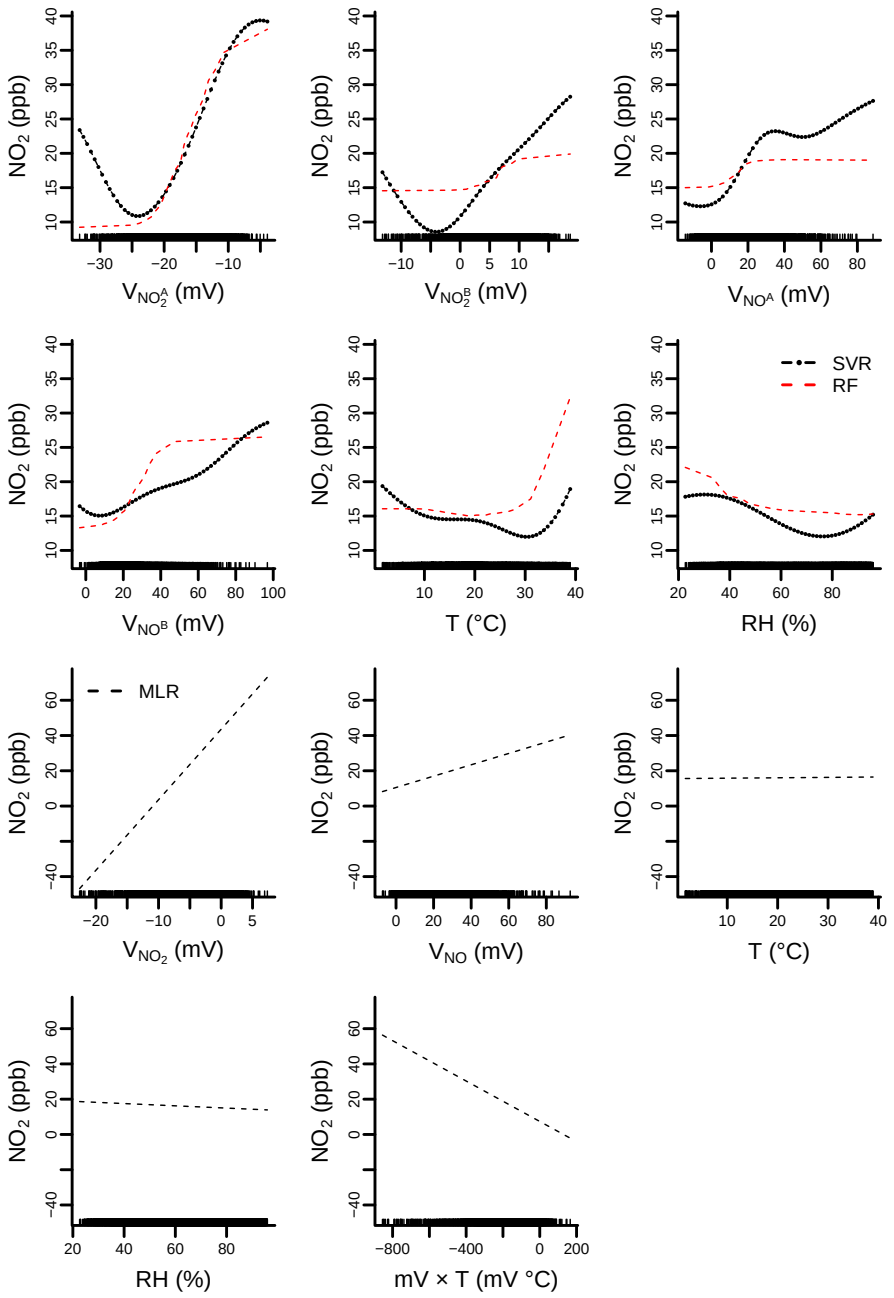

Figure S7: Partial plots for SVM, RF and MLR for the calibration dataset from SU010, NO_2. Rug on the abscissa indicates the range of the covariate.

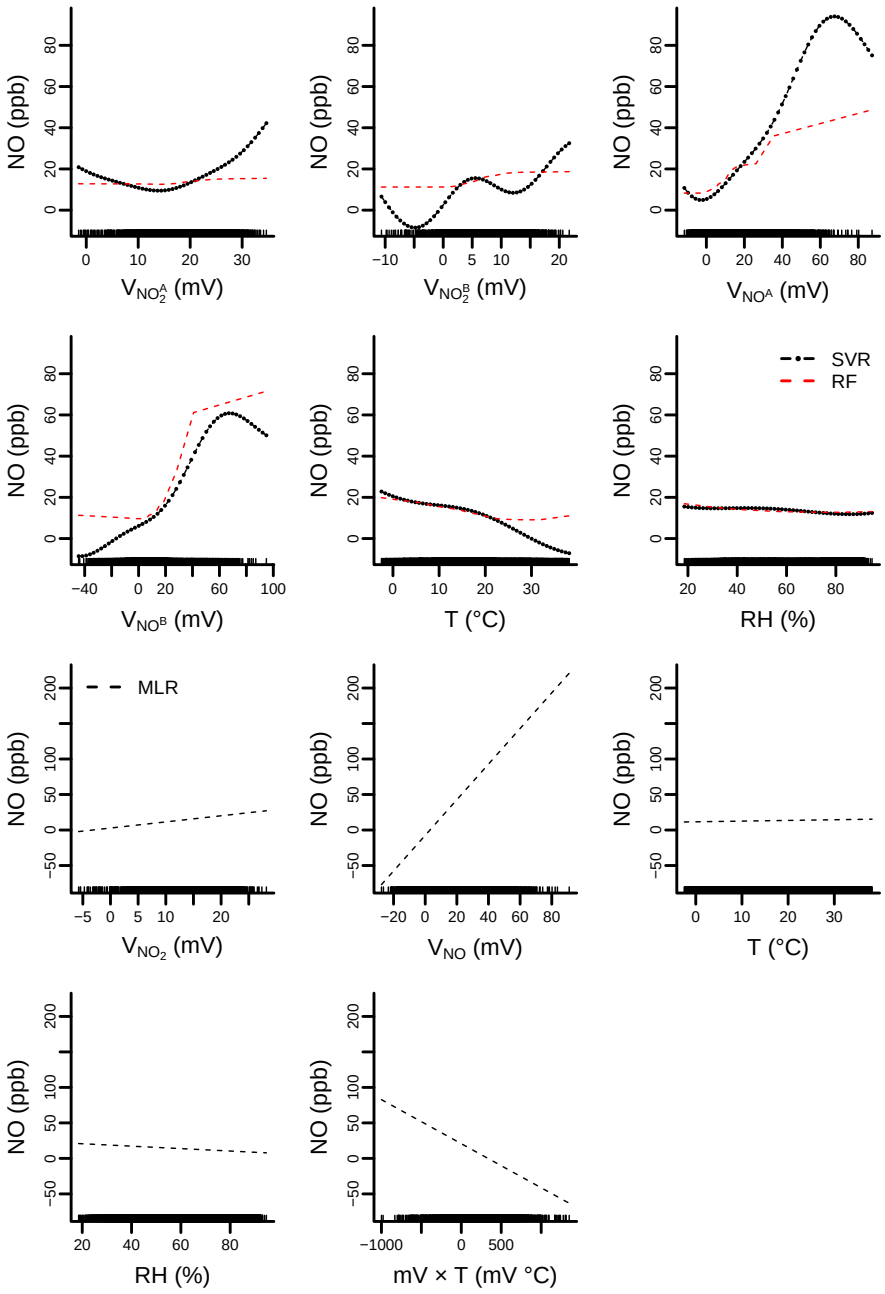

Figure S8: Partial plots for SVM, RF and MLR for the calibration dataset from SU011, NO. Rug on the abscissa indicates the range of the covariate.

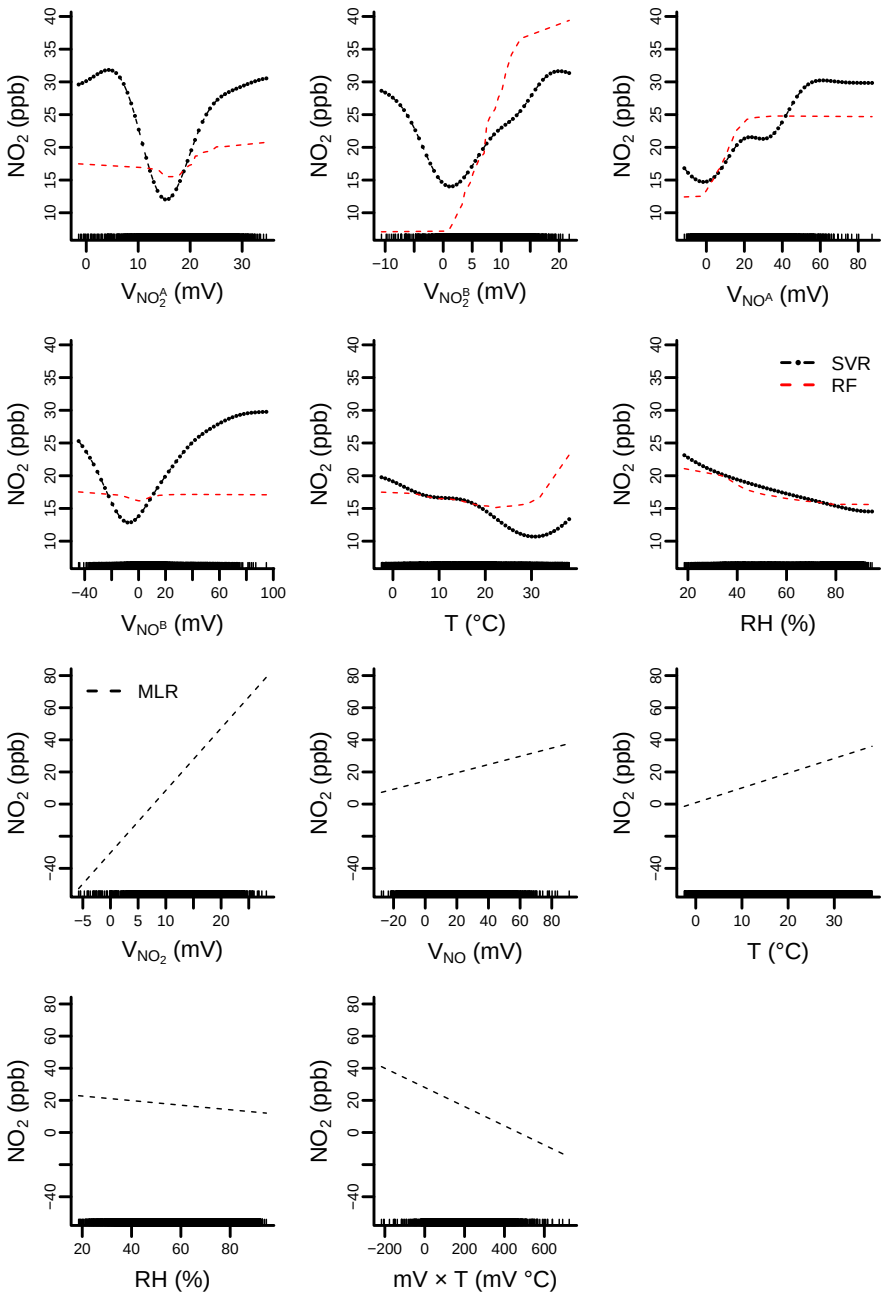

Figure S9: Partial plots for SVM, RF and MLR for the calibration dataset from SU011, NO_2. Rug on the abscissa indicates the range of the covariate.

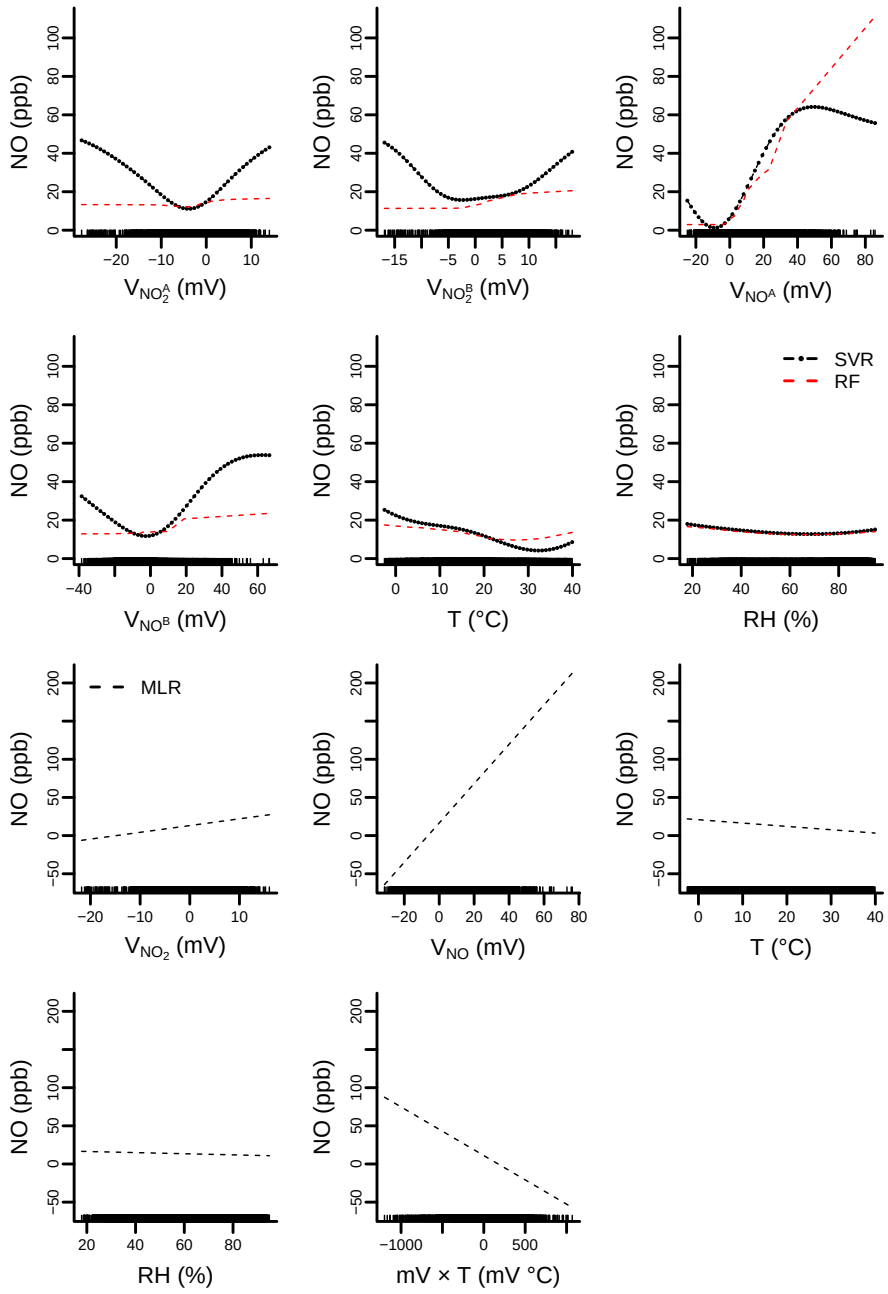

Figure S10: Partial plots for SVM, RF and MLR for the calibration dataset from SU012, NO. Rug on the abscissa indicates the range of the covariate.

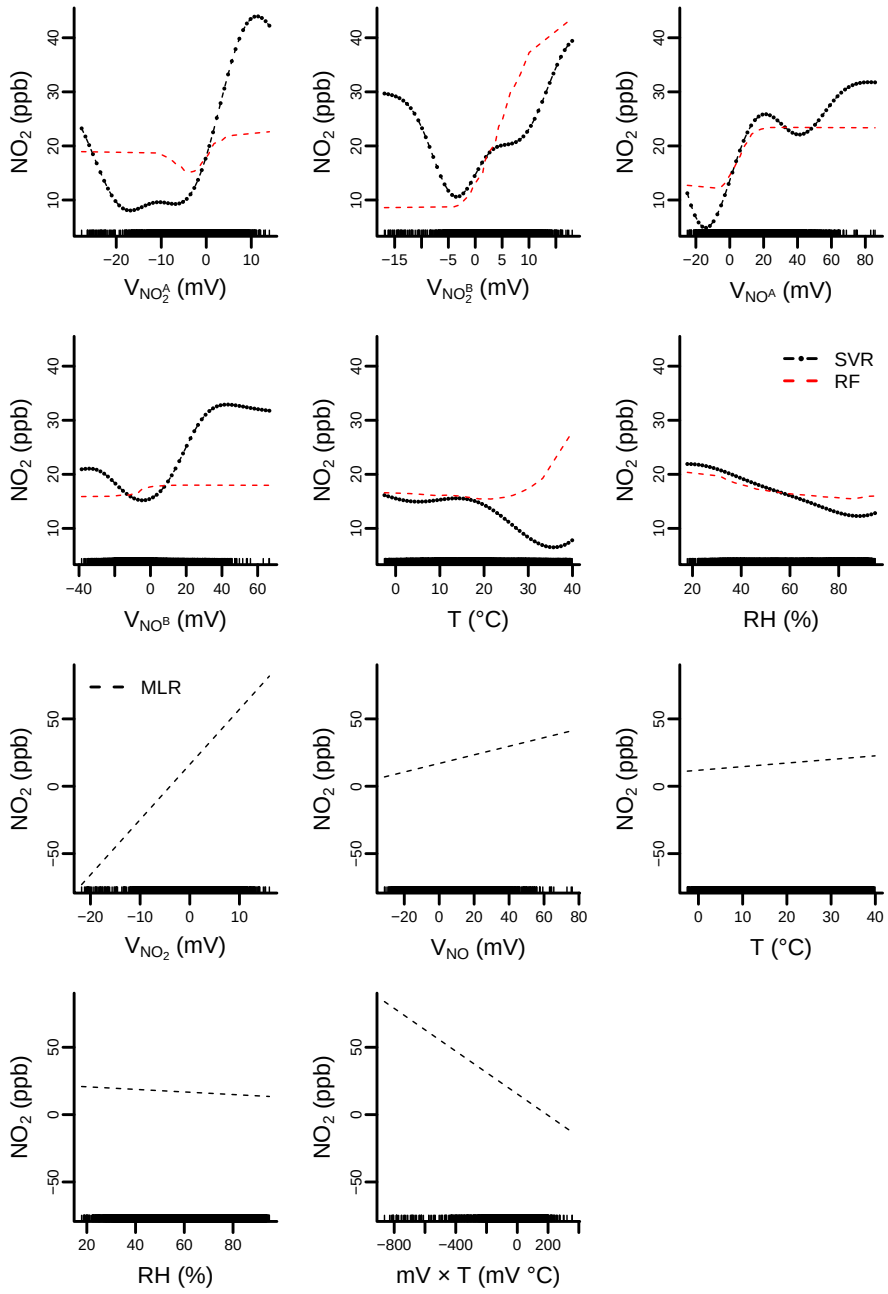

Figure S11: Partial plots for SVM, RF and MLR for the calibration dataset from SU012, NO_2. Rug on the abscissa indicates the range of the covariate.

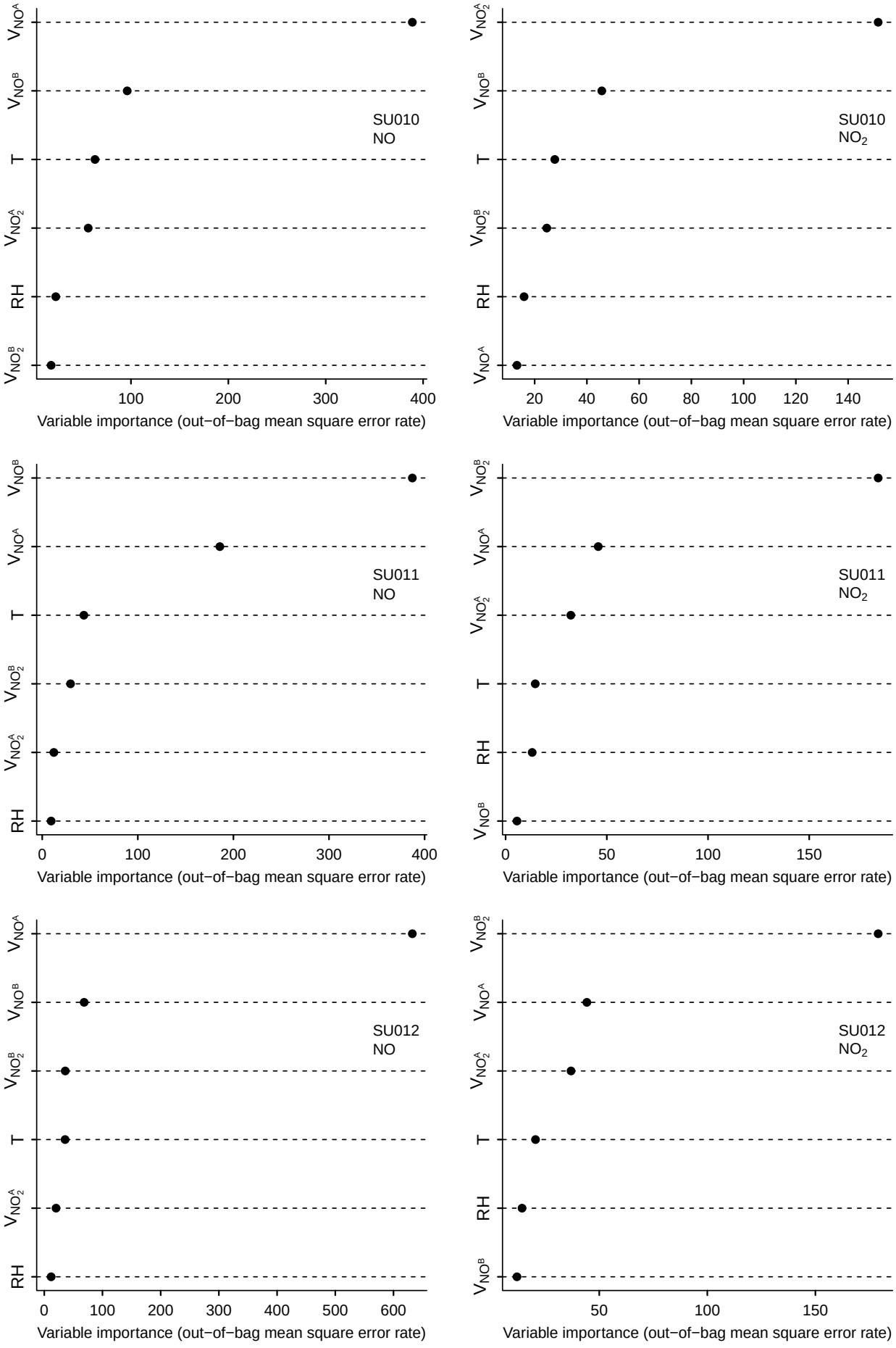

Figure S12: Variable importance plot for the prediction by SU010, SU011 and SU012 of NO and NO_2.

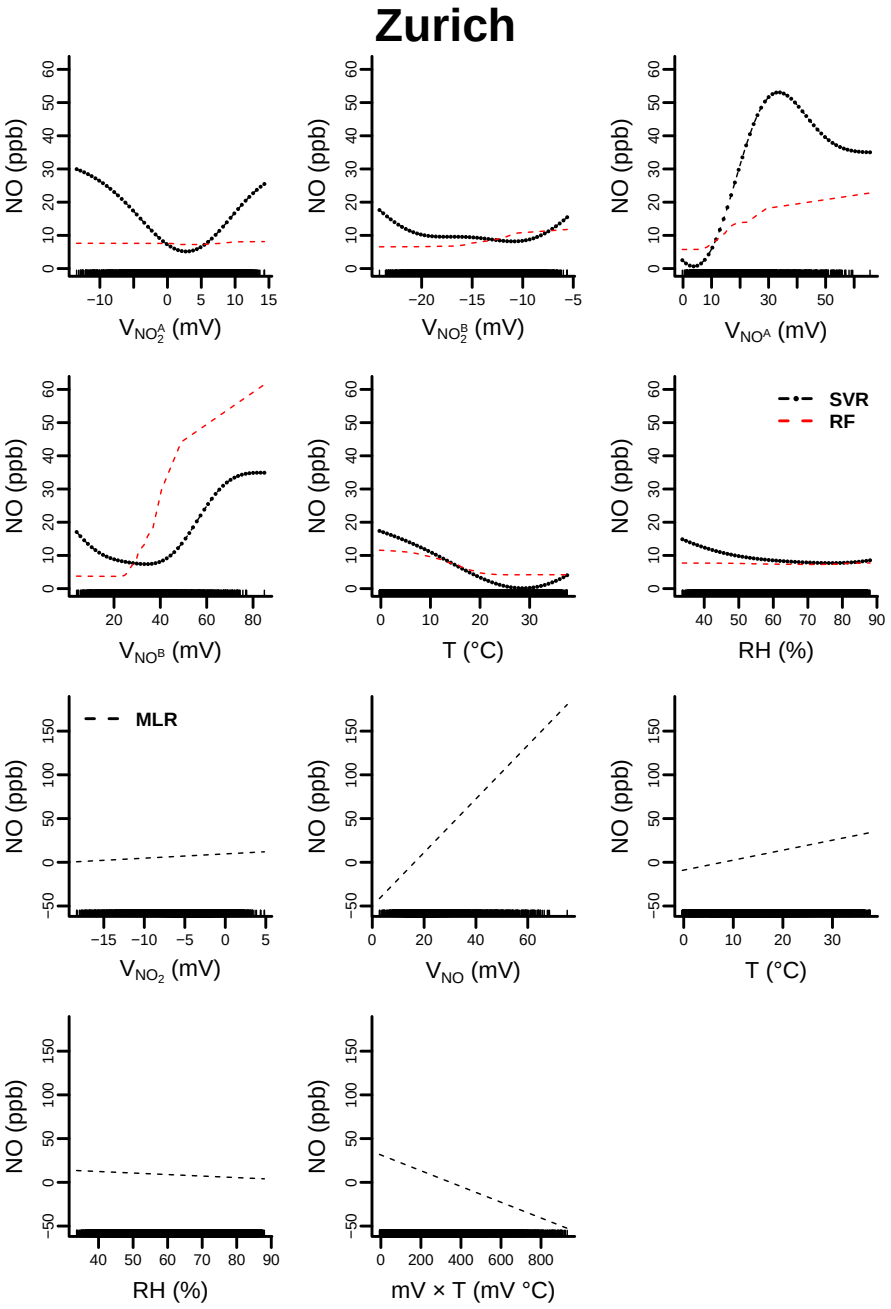

Figure S13: Partial plots for SVM, RF and MLR for the deployment dataset from SU009, NO. Rug on the abscissa indicates the range of the covariate.

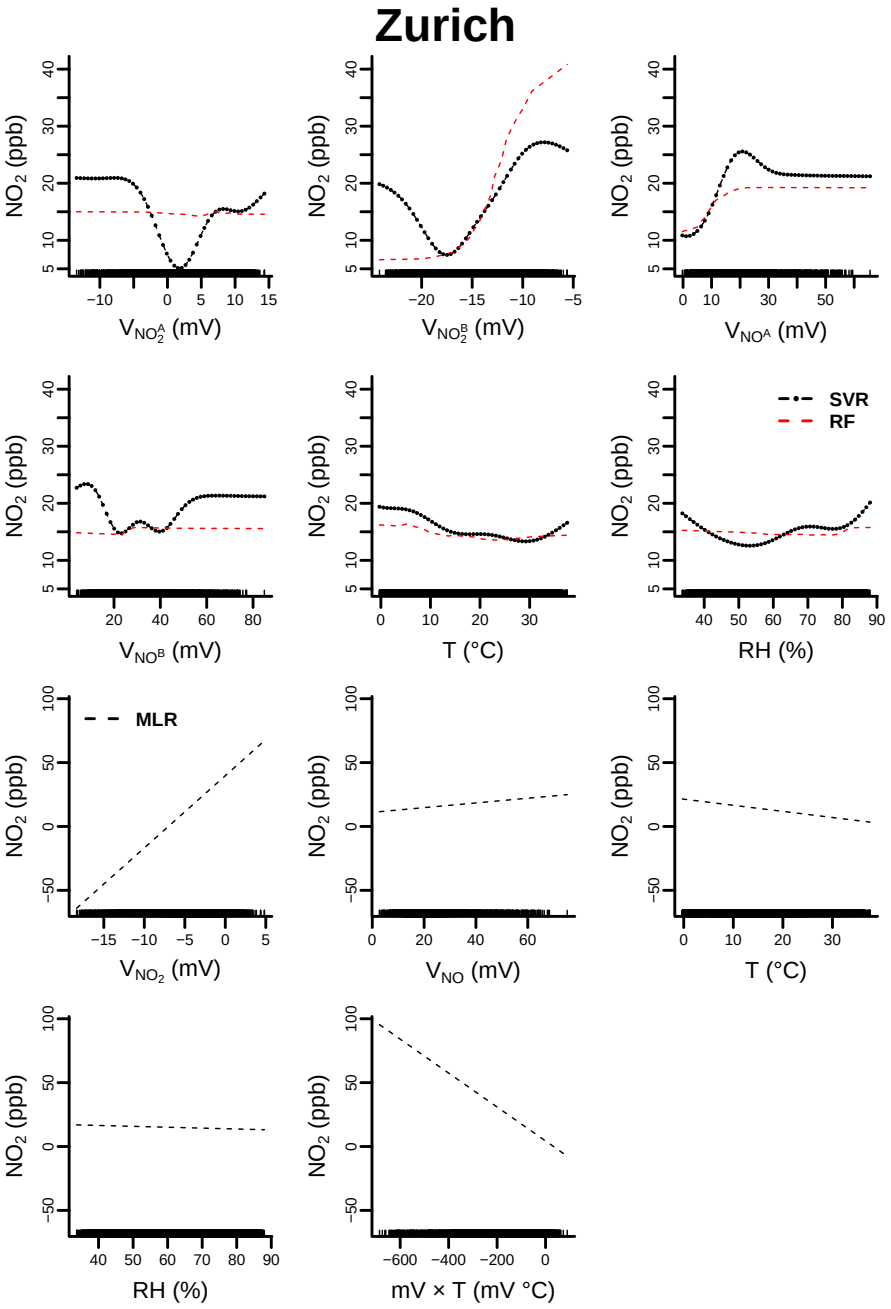

Figure S14: Partial plots for SVM, RF and MLR for the deployment dataset from SU009, NO_2. Rug on the abscissa indicates the range of the covariate.

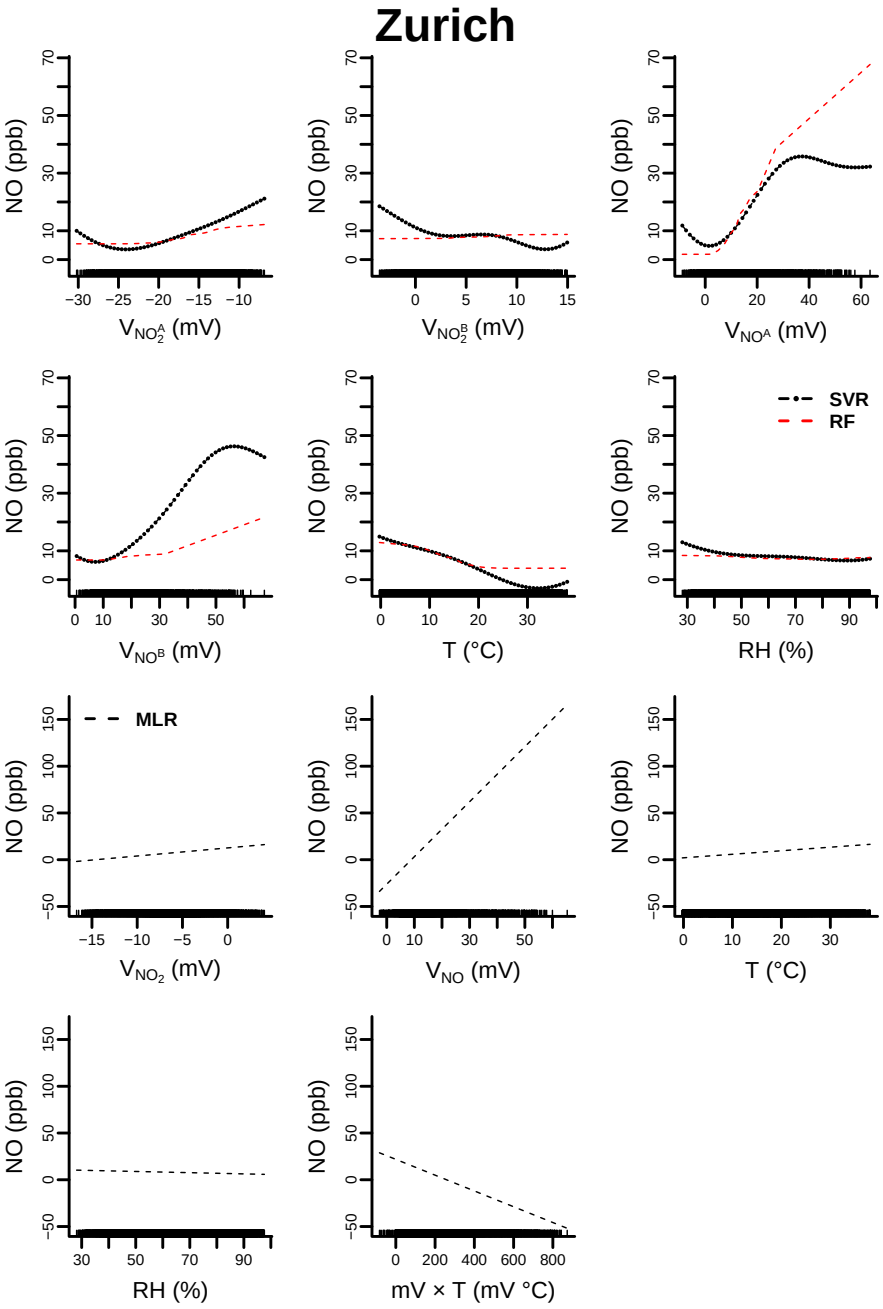

Figure S15: Partial plots for SVM, RF and MLR for the deployment dataset from SU010, NO. Rug on the abscissa indicates the range of the covariate.

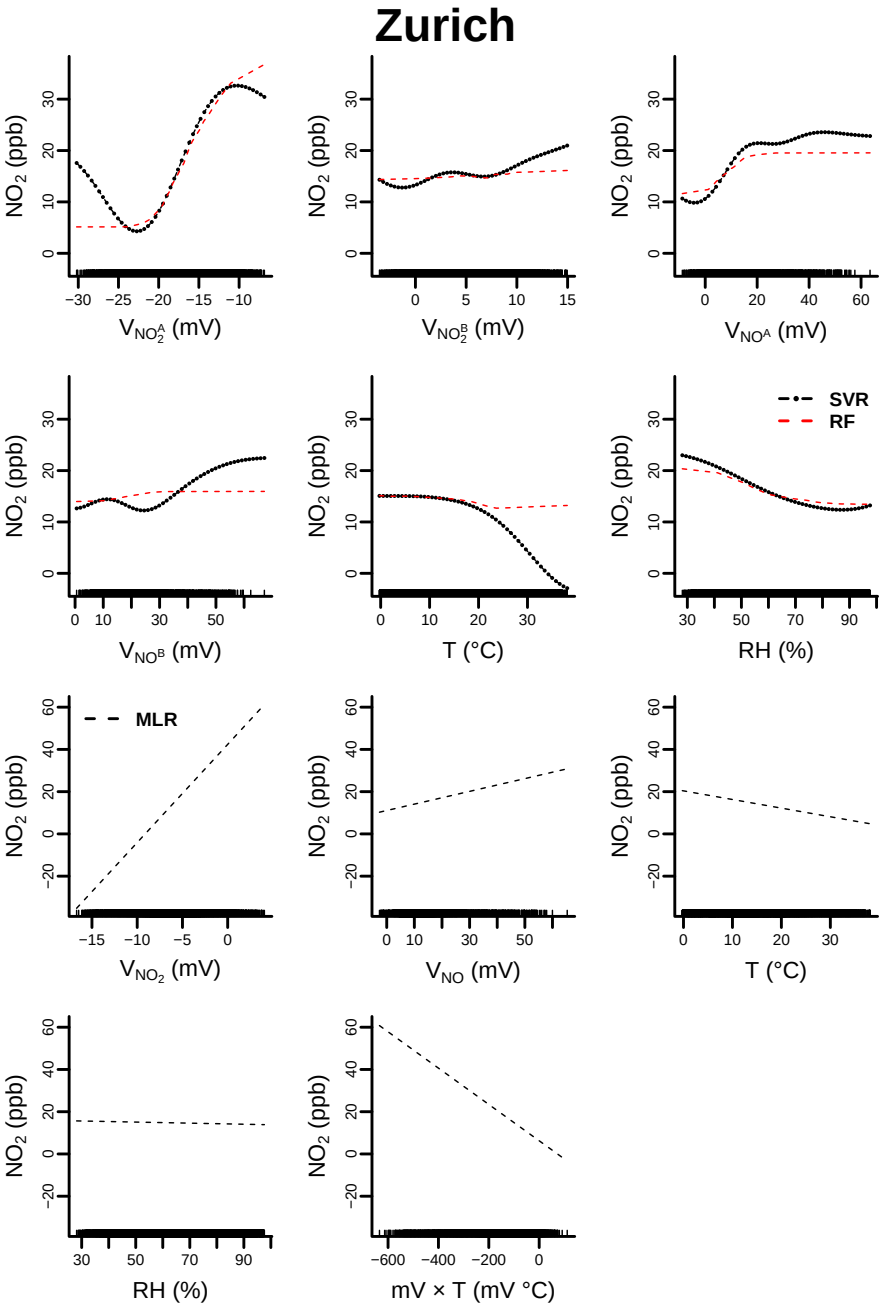

Figure S16: Partial plots for SVM, RF and MLR for the deployment dataset from SU010, NO_2. Rug on the abscissa indicates the range of the covariate.

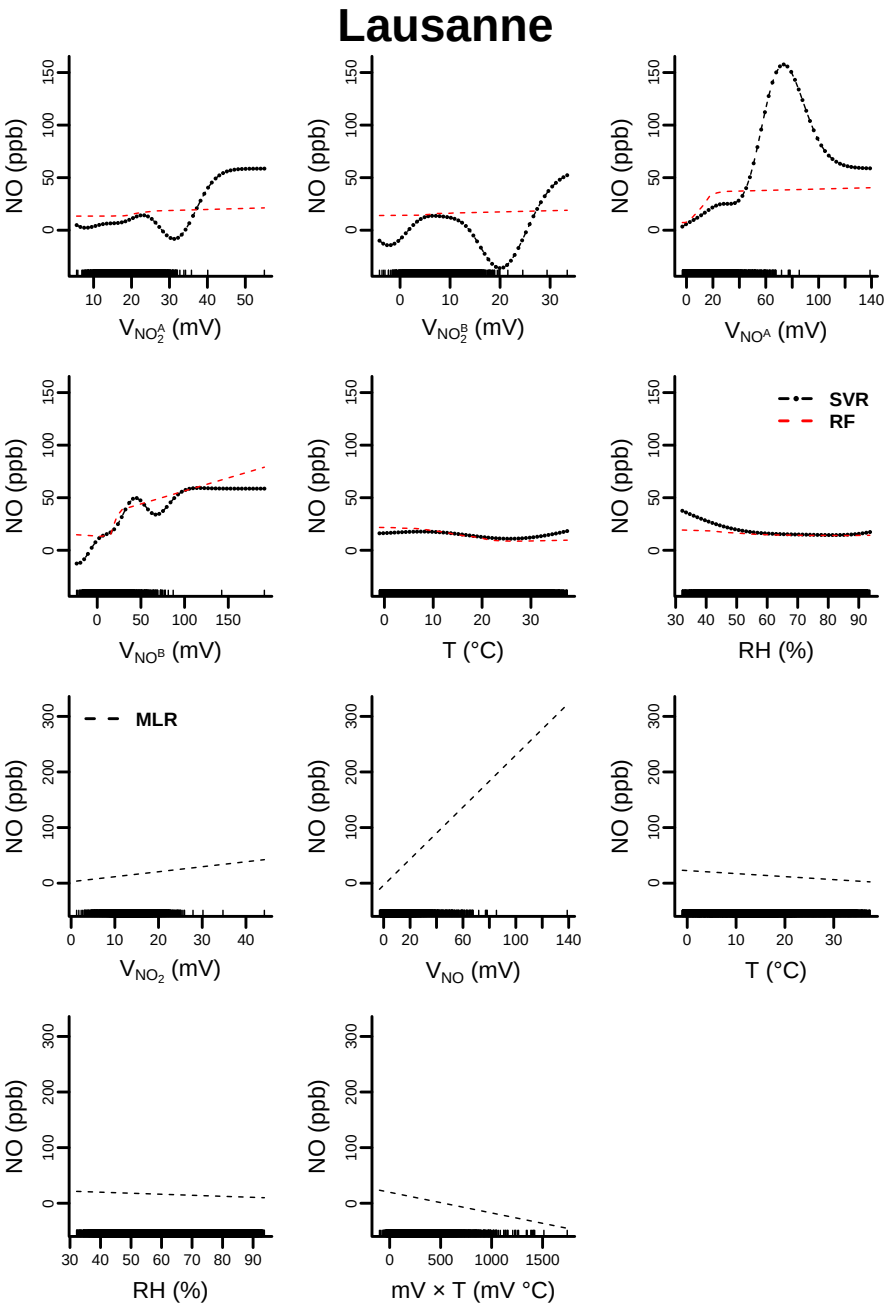

Figure S17: Partial plots for SVM, RF and MLR for the deployment dataset from SU011, NO. Rug on the abscissa indicates the range of the covariate.

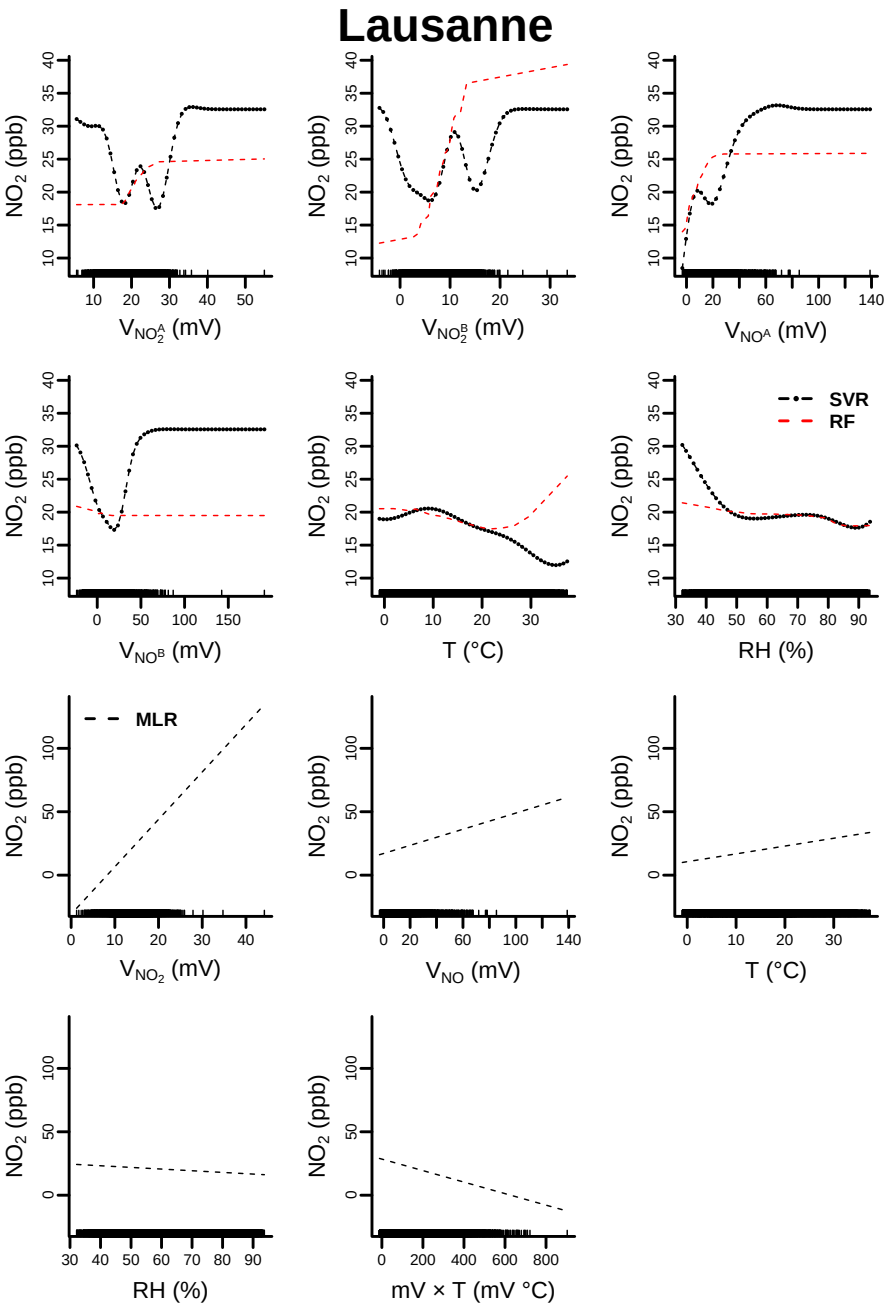

Figure S18: Partial plots for SVM, RF and MLR for the deployment dataset from SU011, NO_2. Rug on the abscissa indicates the range of the covariate.

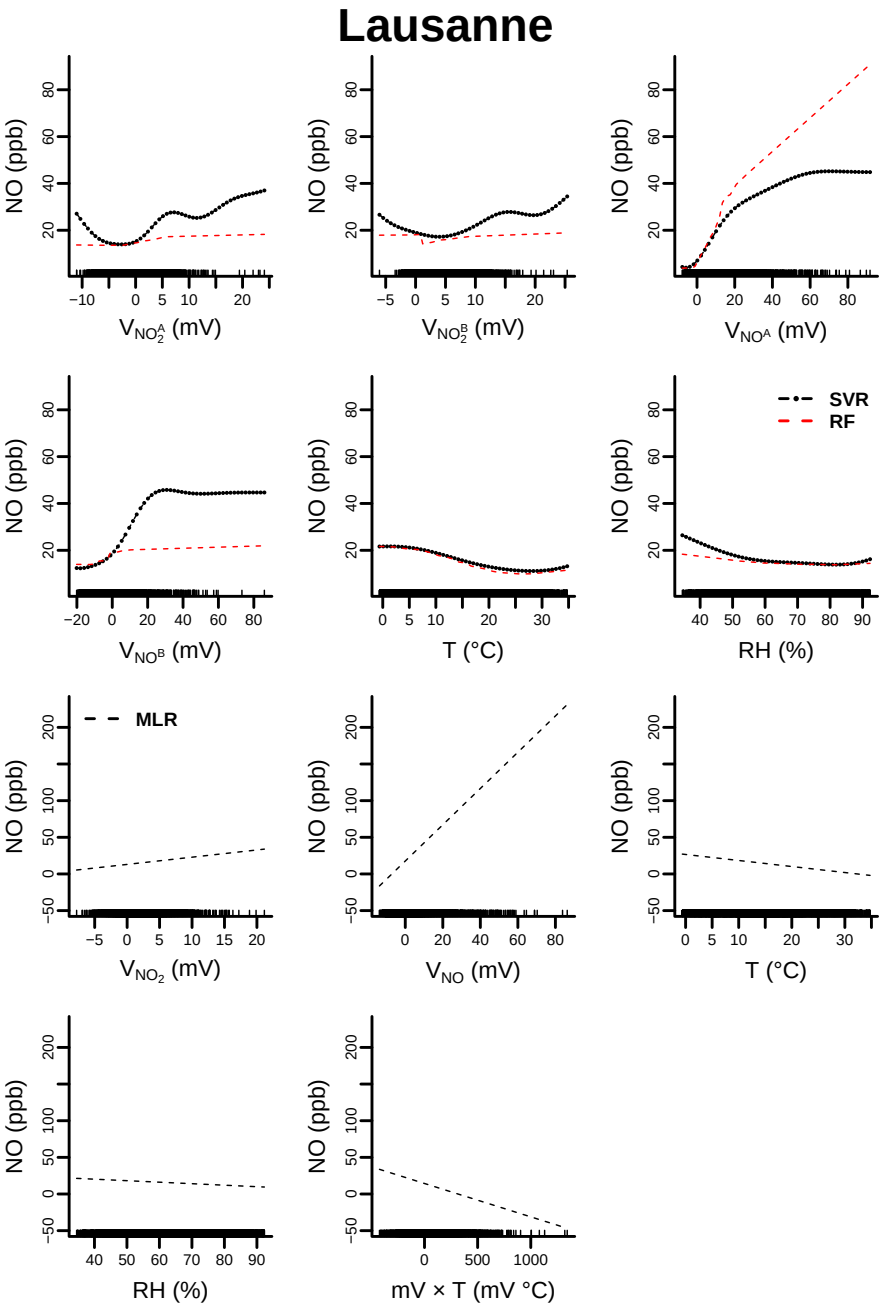

Figure S19: Partial plots for SVM, RF and MLR for the deployment dataset from SU012, NO. Rug on the abscissa indicates the range of the covariate.

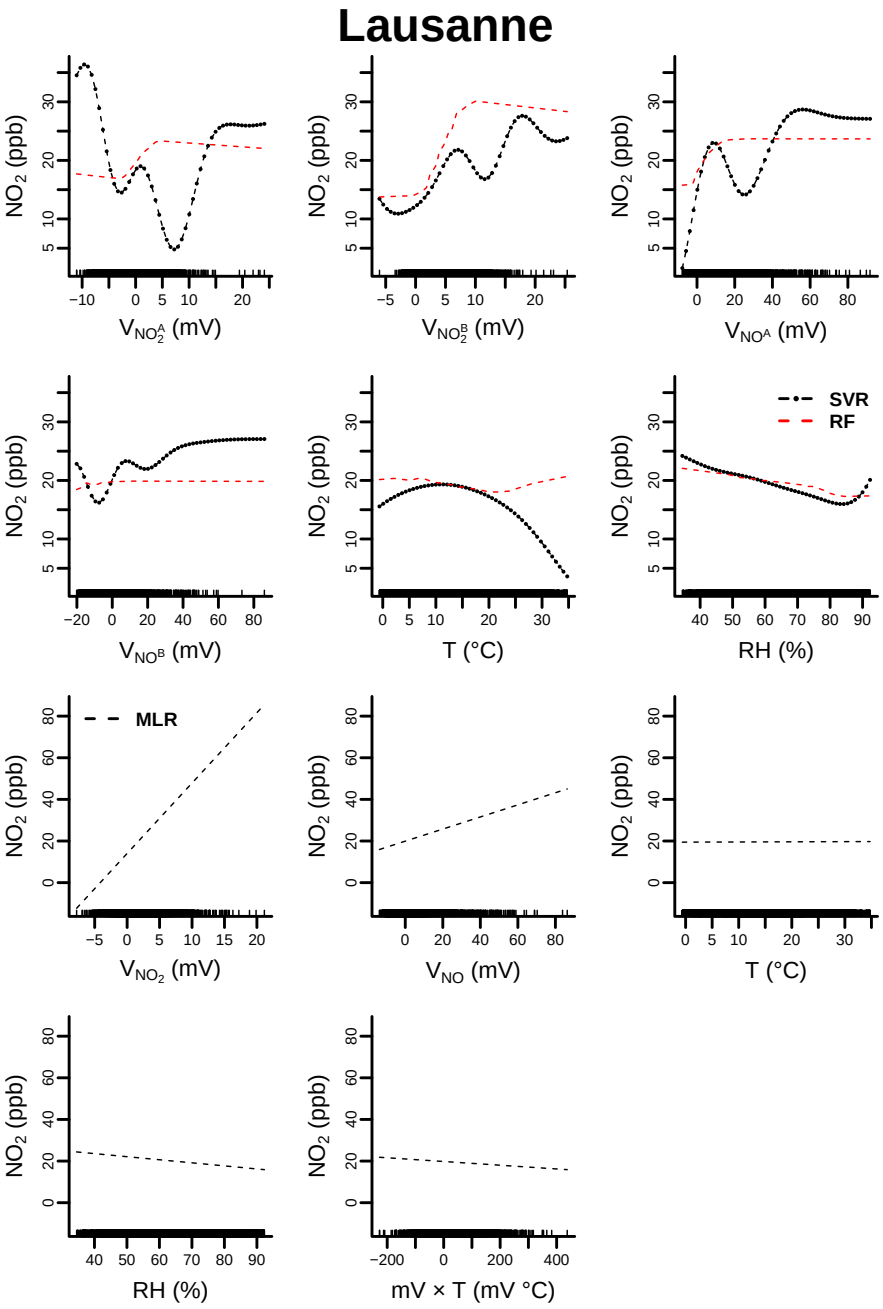

Figure S20: Partial plots for SVM, RF and MLR for the deployment dataset from SU012, NO_2. Rug on the abscissa indicates the range of the covariate.

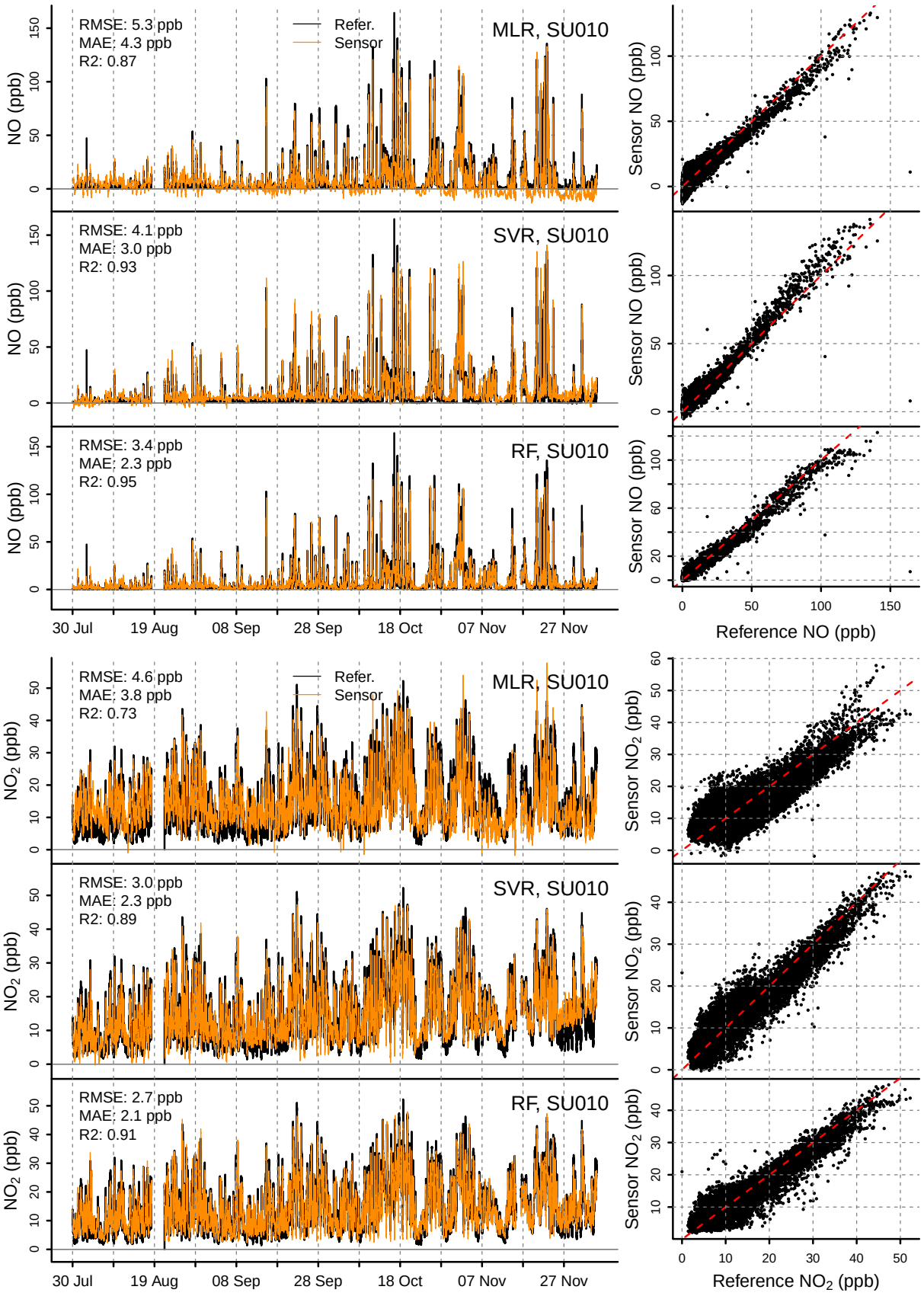

Figure S21: Comparison of NO (top) and NO_2 (bottom) estimates by SU010 with observations by reference instruments, at the urban background site Zurich-Kaserne. 1:1 red dashed line is added in the scatterplots.

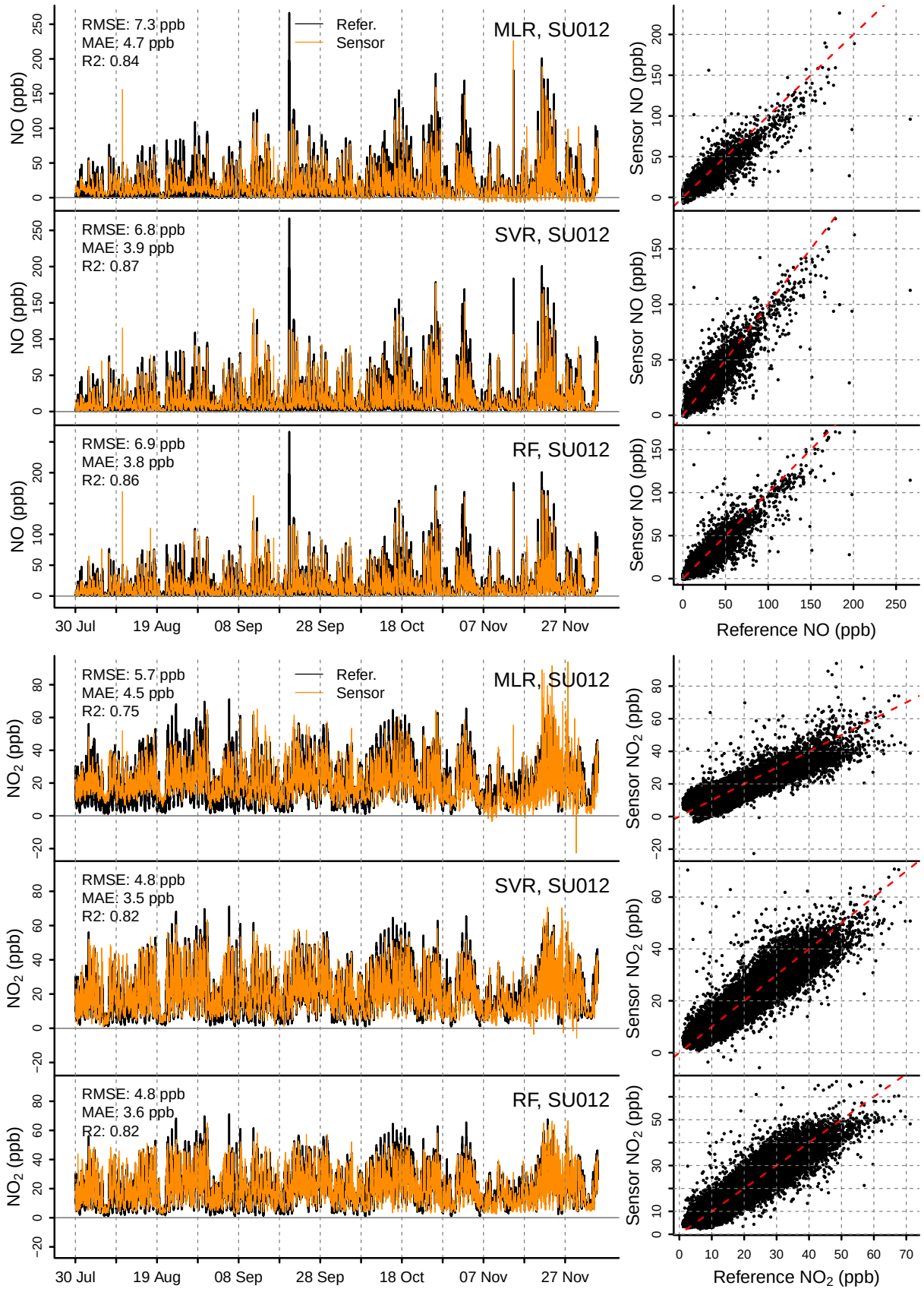

Figure S22: Comparison of NO (top) and NO_2 (bottom) estimates by SU012 with observations by reference instruments, at the urban traffic site of Lausanne. 1:1 red dashed line is added in the scatterplots.

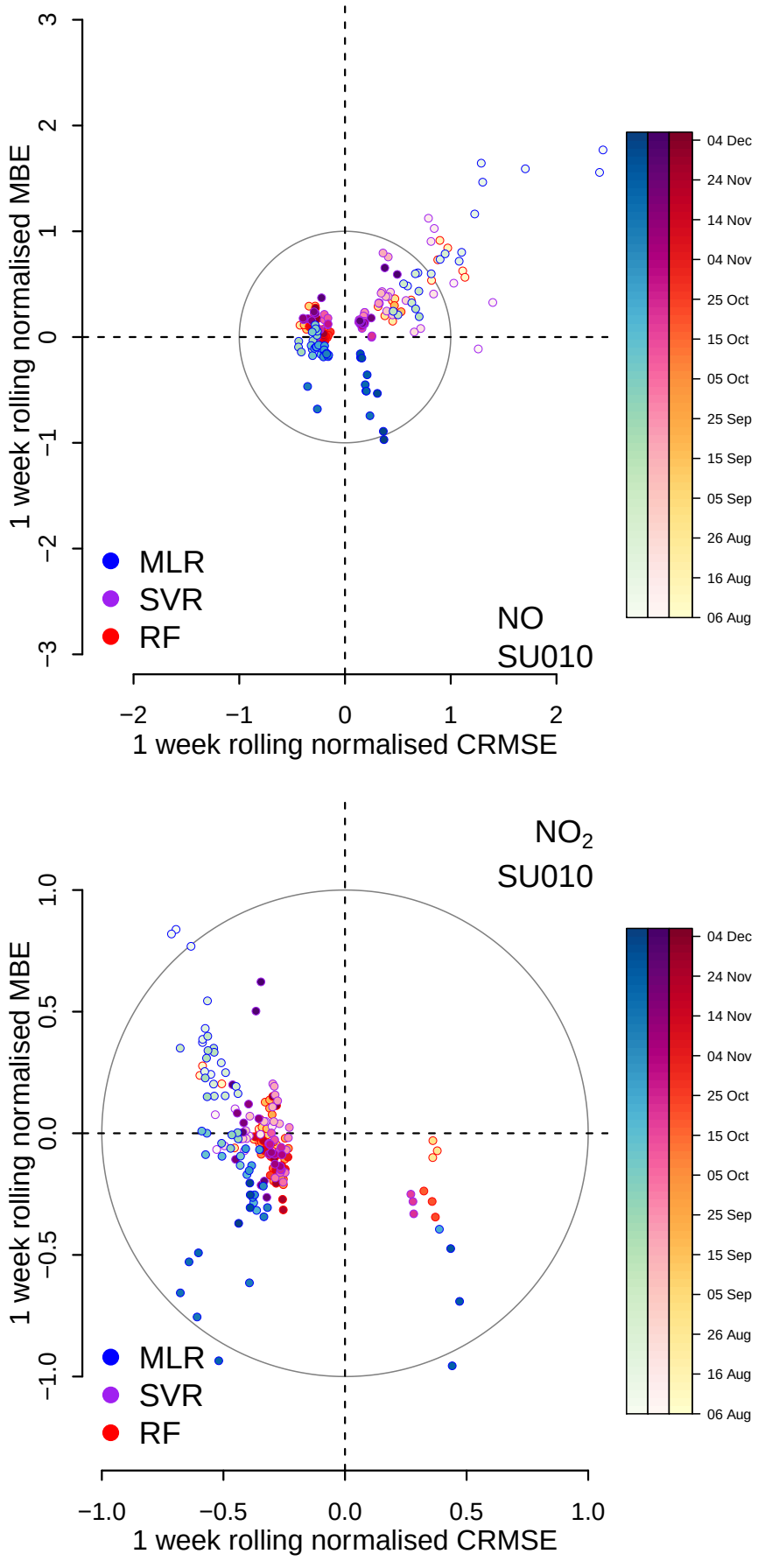

Figure S23: Target plot for the NO (top) and NO_2 (bottom) estimate by SU010, in Zurich urban background.

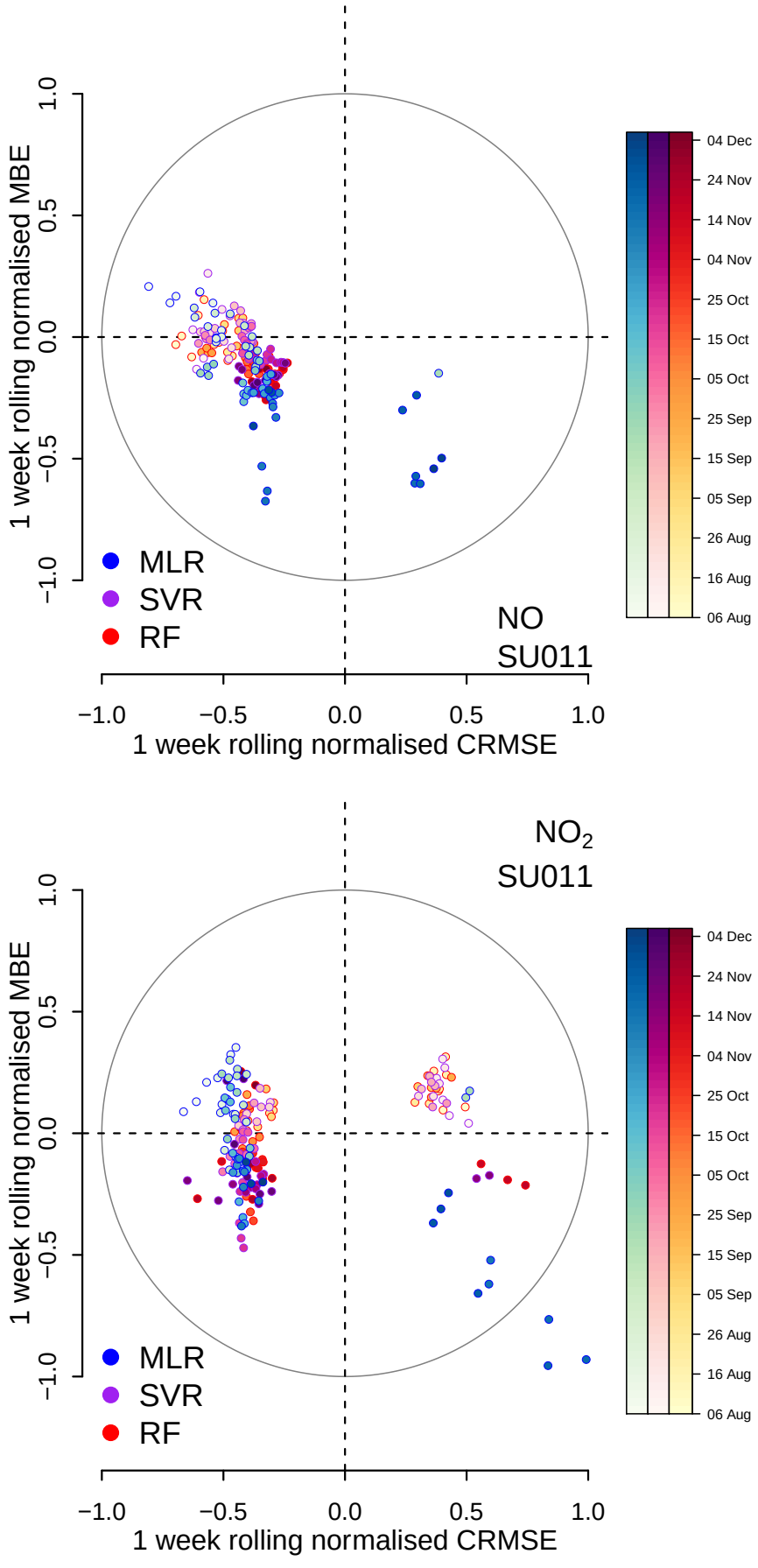

Figure S24: Target plot for the NO (top) and NO_2 (bottom) estimate by SU011, in Lausanne urban traffic.

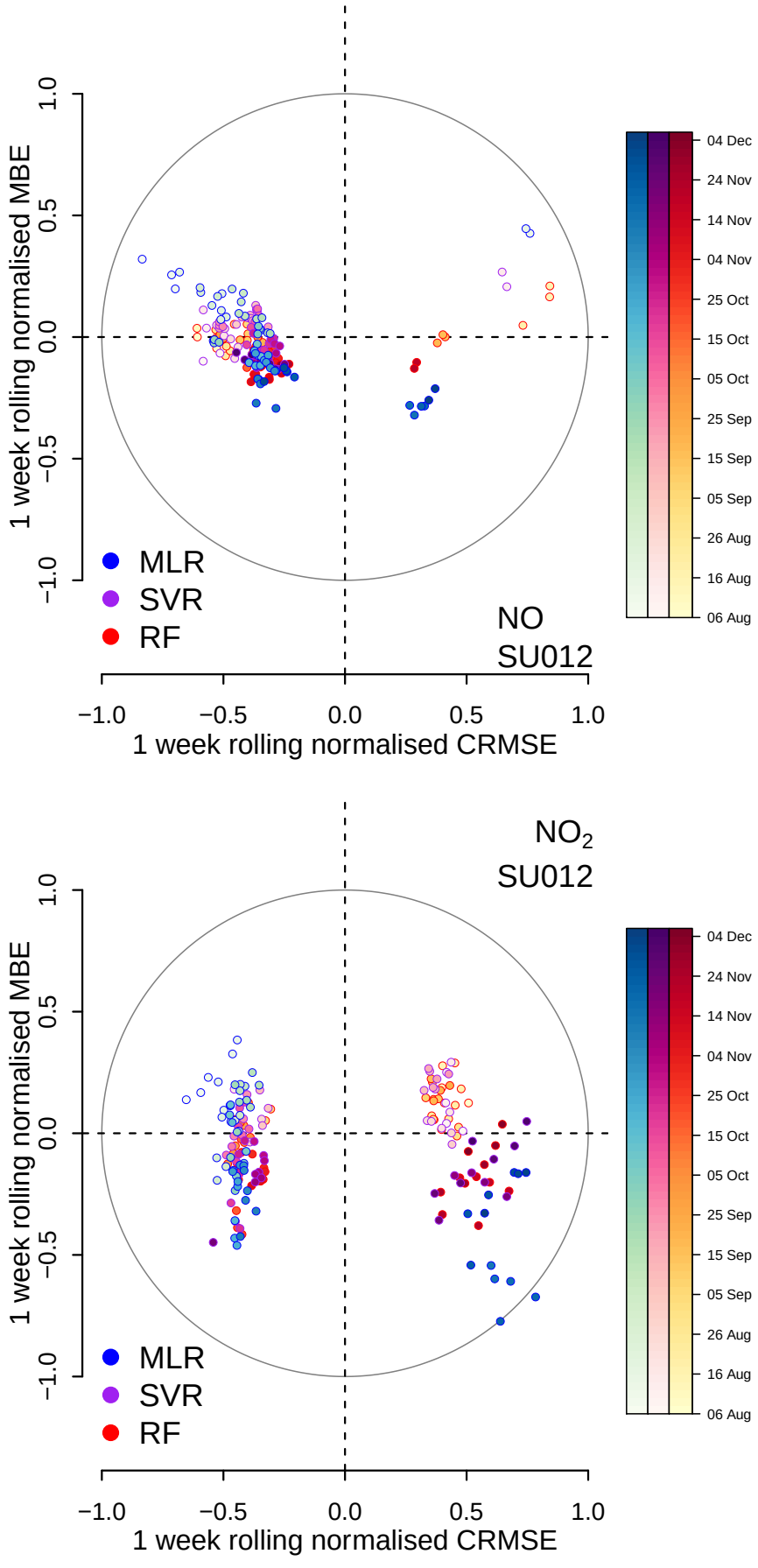

Figure S25: Target plot for the NO (top) and NO_2 (bottom) estimate by SU012, in Lausanne urban traffic.

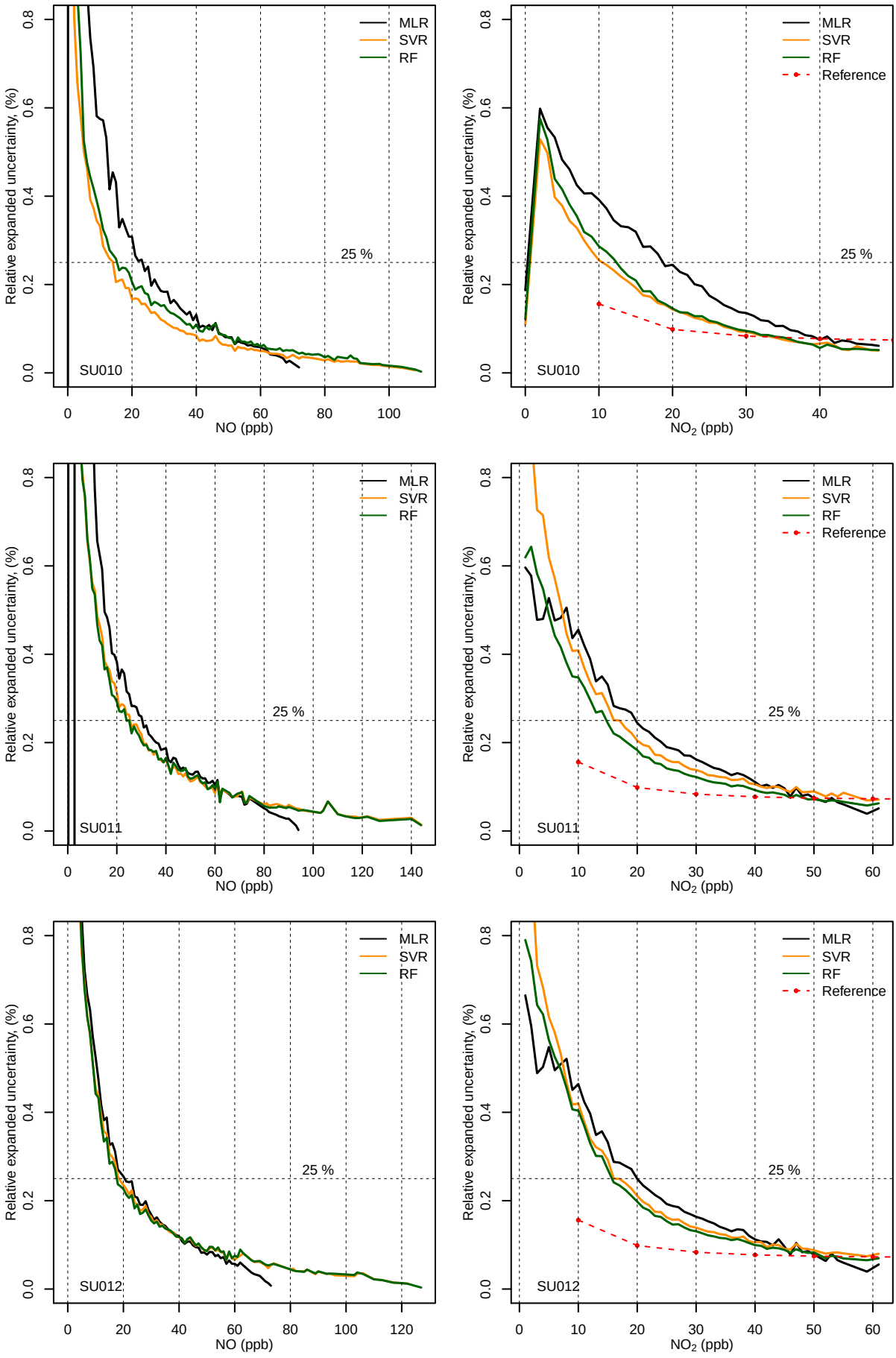

Figure S26: Comparison of expanded relative uncertainty and reference NO and NO_2 concentration for the SU010, SU011 and SU012, using 1 hour average data.

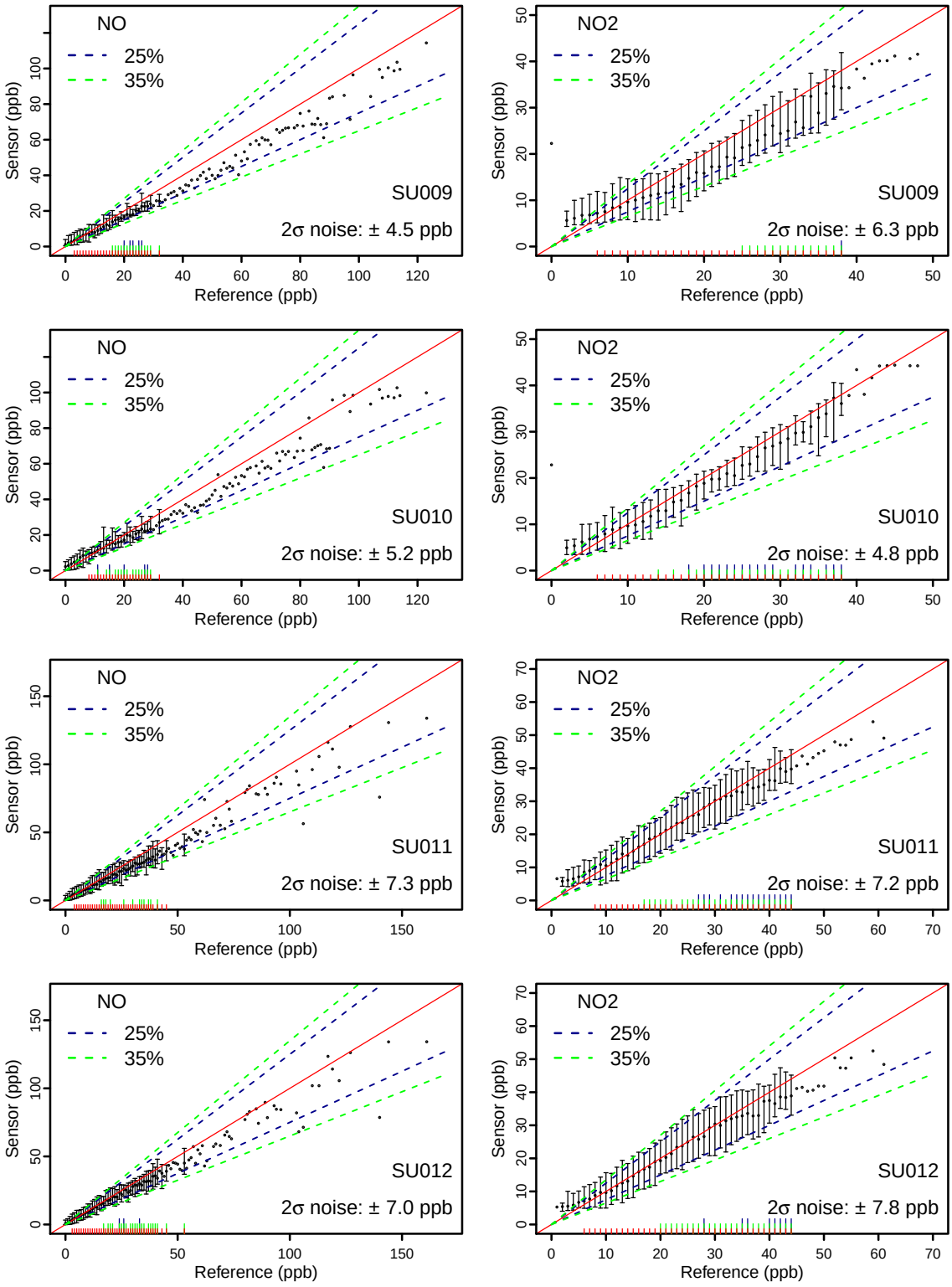

Figure S27: Range of the output using RF algorithm at the deployment sites. The reference data were binned by 1 ppb concentration interval. For each bin the median of the concentration estimated by the sensing device. When at least 10 readings were available, the 5th and 95th quantiles were included. 1:1 dashed line is added, along with its 25% and 35% uncertainty bands. Bottom red rug indicates if the median of sensor estimate is included in the in the 25% uncertainty bounds. Bottom green (blue) rug indicates if the 5 – 95% percentile range of estimates is included in the 35% (25%) uncertainty range.

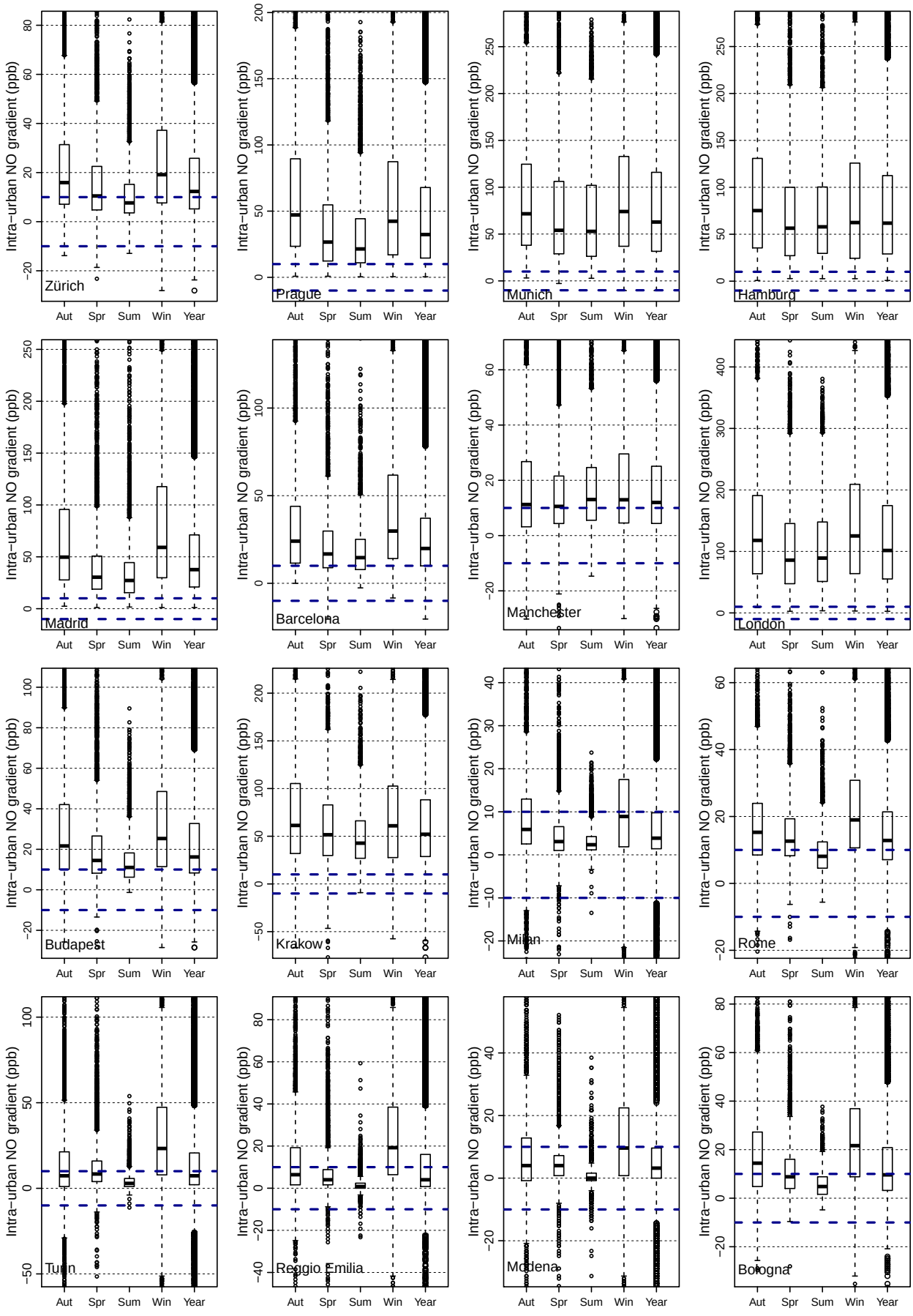

Figure S28: Seasonal boxplots of intra–urban NO gradient in a pool of European cities, proceeding from the station pairs having the largest difference in NO, on a hourly basis. Blue dashed lines indicate ± 10 ppb.

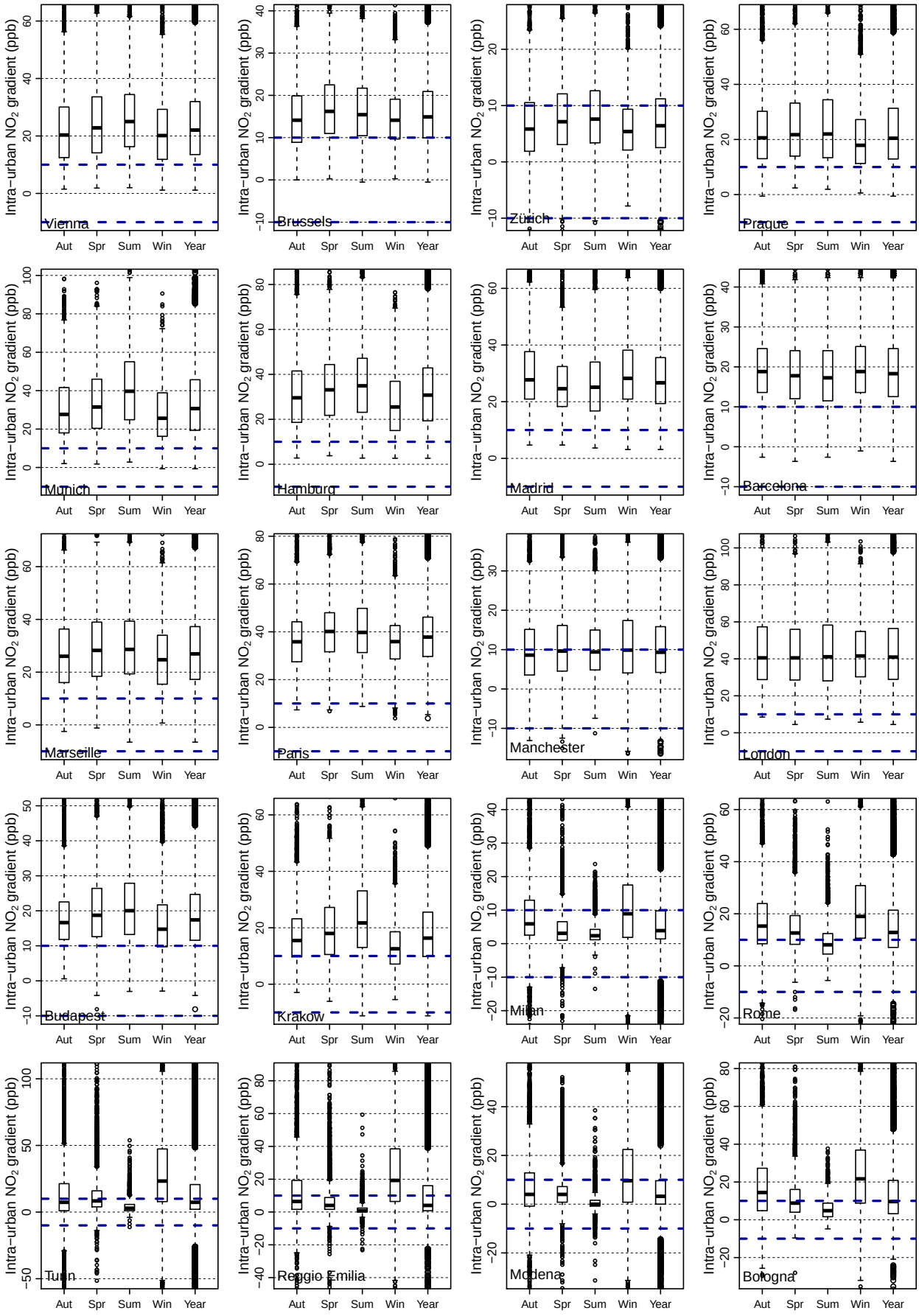

Figure S29: Seasonal boxplots of intra–urban NO_2 gradient in a pool of European cities, proceeding from the station pairs having the largest difference in NO_2, on a hourly basis. Blue dashed lines indicate ± 10 ppb.

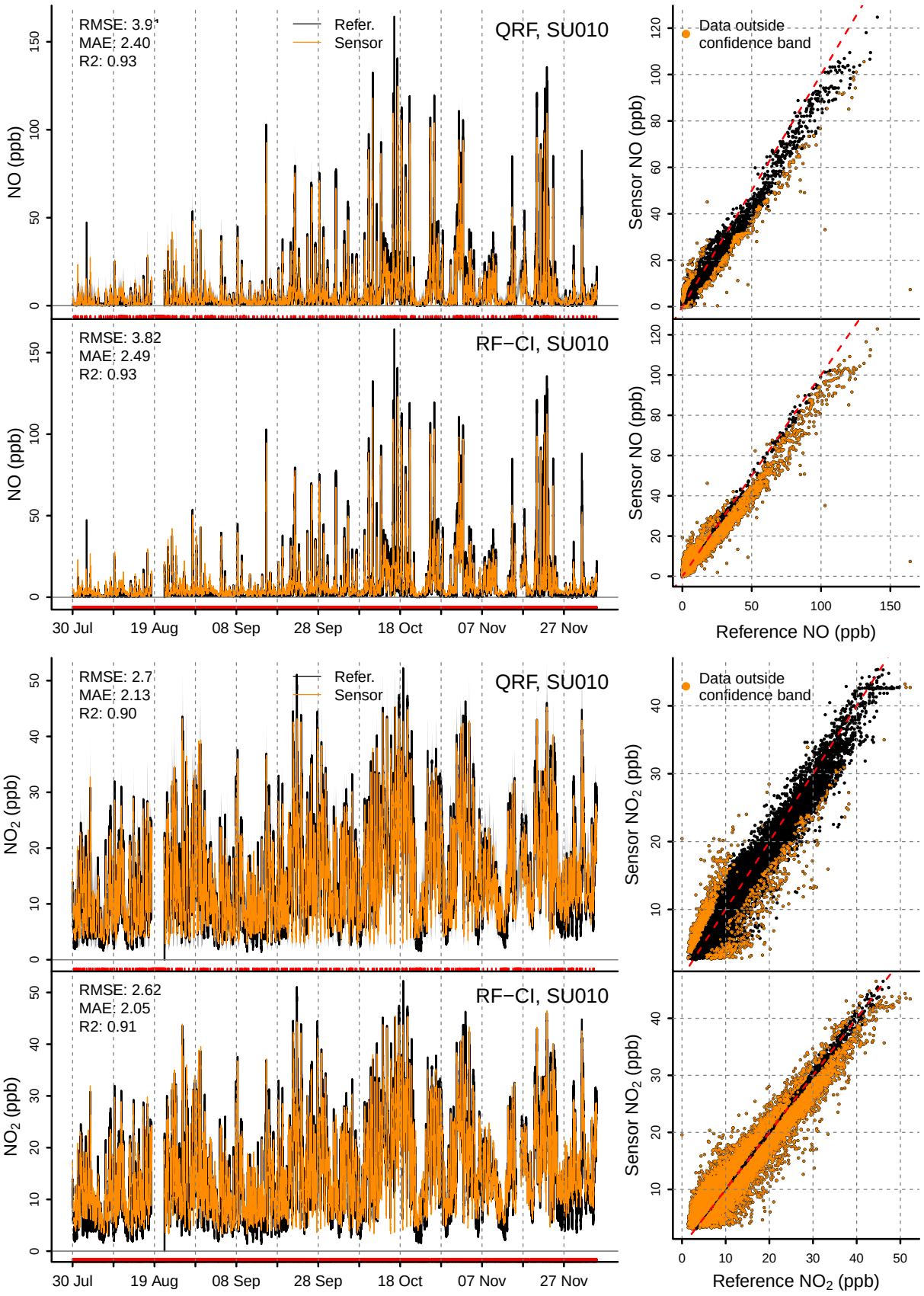

Figure S30: Comparison of QRF and CI-RF estimates of NO (top) and NO_2 (bottom) by SU010 with observations by reference instruments. 1:1 red dashed line is added in the scatterplots.

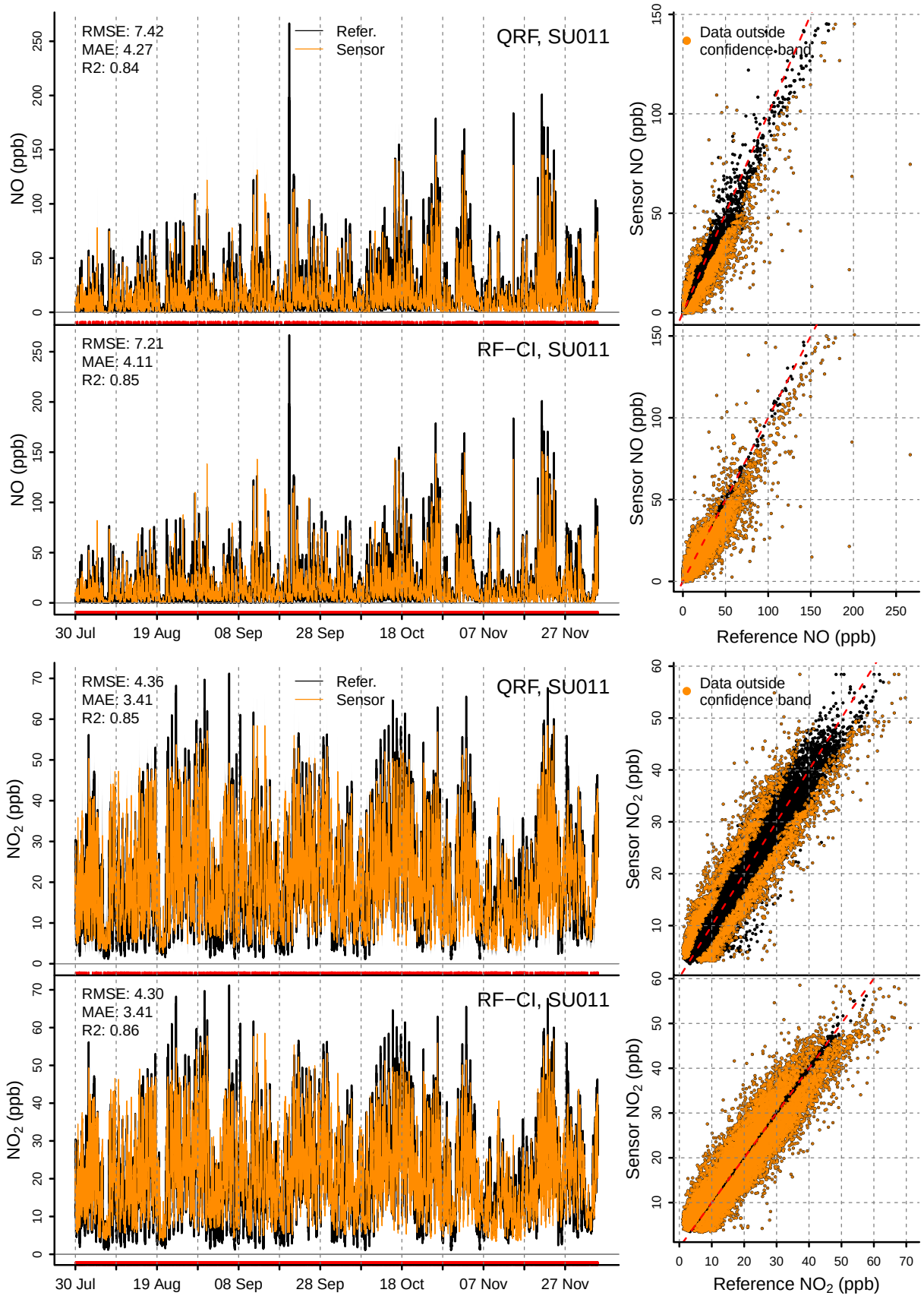

Figure S31: Comparison of QRF and CI-RF estimates of NO (top) and NO_2 (bottom) by SU011 with observations by reference instruments. 1:1 red dashed line is added in the scatterplots.

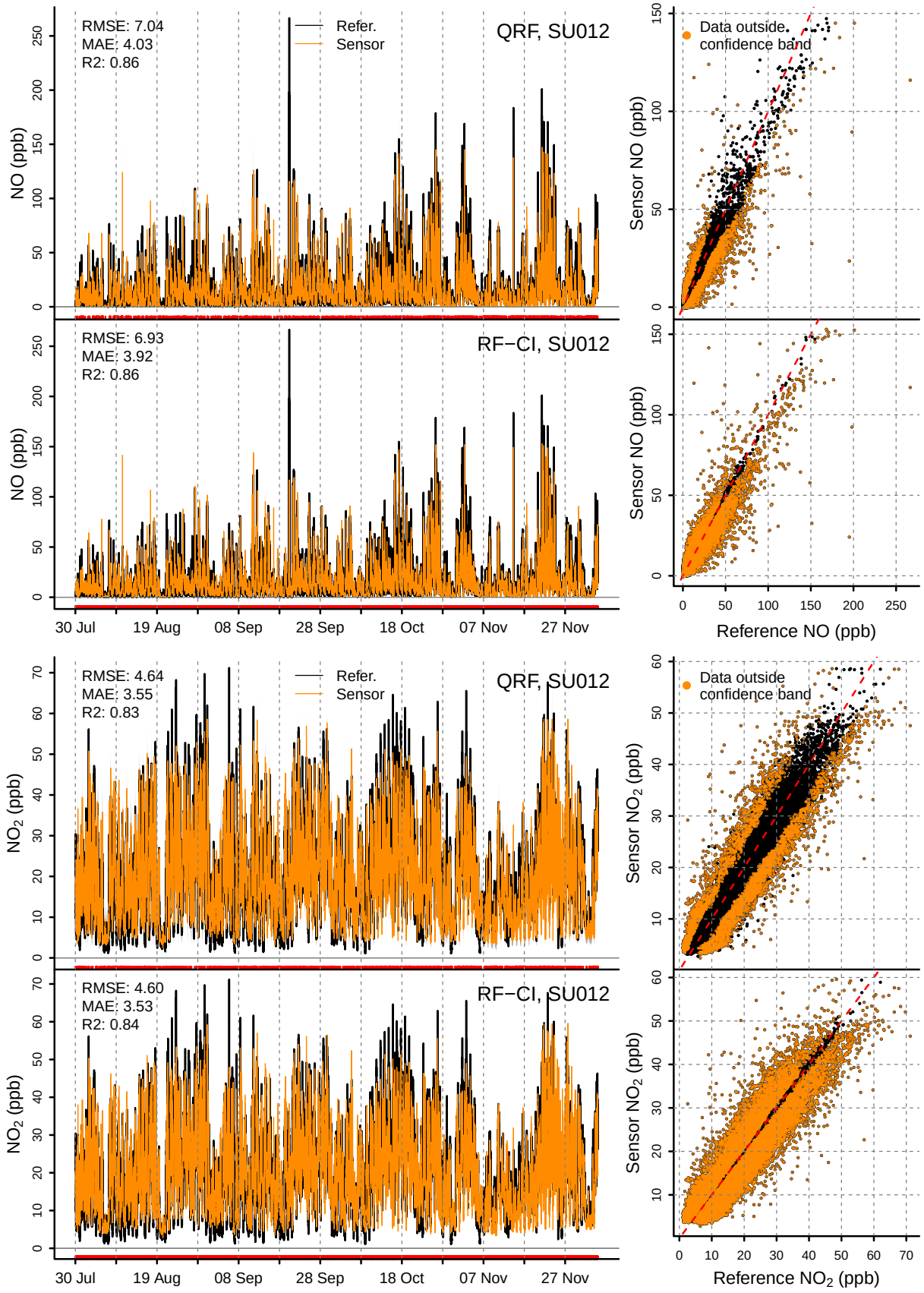

Figure S32: Comparison of QRF and CI-RF estimates of NO (top) and NO_2 (bottom) by SU012 with observations by reference instruments. 1:1 red dashed line is added in the scatterplots.